Carbon 155 (2019) 706–726

Contents lists available at ScienceDirect

Carbon

journal homepage: www.elsevier.com/locate/carbon

Review article

Biomass derived carbon as binder-free electrode materials for supercapacitors

Yulin Wang [a, d], Qingli Qu [a, d], Shuting Gao [a, d], Guosheng Tang [a, b], Kunming Liu [c], Shuijian He [b, *], Chaobo Huang [a, d, **]

[a] College of Chemical Engineering, Jiangsu Co-Innovation Center of Efficient Processing and Utilization of Forest Resources, Nanjing Forestry University, Nanjing, 210037, PR China
[b] College of Materials Science and Engineering, Nanjing Forestry University, Nanjing 210037, China
[c] School of Metallurgical and Chemical Engineering, Jiangxi University of Science and Technology, Ganzhou 341000, China
[d] Laboratory of Biopolymer based Functional Materials, Nanjing Forestry University, Nanjing, 210037, PR China

ARTICLE INFO

Article history:
Received 29 July 2019
Received in revised form
26 August 2019
Accepted 5 September 2019
Available online 6 September 2019

ABSTRACT

Supercapacitors (SCs) with excellent electrochemical properties are considered as potential energy storage devices in applications of increasing power demands. Carbonaceous materials with the developed specific surface area (SSA) and abundant porous structure, are frequently combined with other carbon materials or directly used as electrode material for SCs. Renewable resources of biomass are commonly utilized as carbon precursors owing to their low-cost, easy availability, facile preparation, and environmentally friendly. This article reviews the progress in renewable resources based free-standing electrode materials on the application of supercapacitors. After a concise introduction of SCs, the methodologies on enhancement of the electrochemical performance and obtaining self-supported carbon materials are discussed. Then biomass-based binder-free electrode materials with designed unique architecture for high performance SCs are highlighted. Finally, the challenges associated with biomass derived free-standing carbon materials are pointed out and strategies to meet the practical application of supercapacitors in advanced energy storage systems are discussed. It is expected that this review would inspire researchers with new ideas to promote progress in the field.

Contents

* Corresponding author.
** Corresponding author. College of Chemical Engineering, Jiangsu Co-Innovation Center of Efficient Processing and Utilization of Forest Resources, Nanjing Forestry University, Nanjing, 210037, PR China.
E-mail addresses: shuijianhe86@gmail.com (S. He), haungchaobo@njfu.edu.cn (C. Huang).

https://doi.org/10.1016/j.carbon.2019.09.018
0008-6223/

1. Introduction

In the past few decades, fossil resources have been widely applied in various fields such as automotive industries, agriculture, electricity and transportation. However, due to the overuse of fuels, the global warming is getting worse and fuel reservoirs reduce urgently. Developing renewable resources based cleaner energy storage and conversion devices like solar cells, lithium ion batteries (LIB) and SCs, is regarded as an alternative method to avoid excessive consuming of fossil fuels [1–4]. Supercapacitor has been considered as one of the most potential candidates for applications of fast energy and power supply in last years [5–12].

1.1. Fundamental of supercapacitors

Supercapacitors, also named electrochemical capacitors or ultracapacitors, have caught the intensive attractions as energy storage devices, which bridge the gap between conventional dielectric capacitor and LIB [13,14]. Actually, the charge of rechargeable batteries mainly derives from the intercalation/de-intercalation of cations. Therefore, it is mainly regulated by the diffusion control of ions. But, this phenomenon remarkably restricts the charge/discharge rate of LIB [15]. Due to their higher power capacity, longer cycling stability compared with LIB, and better energy density than dielectric capacitors, SCs with higher safety are typically considered as the alternative to batteries in demand of high power delivery applications [16–18]. Until now, the newly developed SCs have been applied in hybrid electric vehicles, regenerative brakings, powercache and uninterruptible power supply, etc. [13,19,20].

Supercapacitors are generally divided into two classes by charge storage mechanisms, including electrochemical double-layer capacitors (EDLCs) and pseudo-capacitors (PCs) [21]. The former refers to the physical phenomena of electrostatic storage occurring at the electrode-electrolyte interface [14,22,23]. EDLCs depend on the rapid and reversible ion adsorption/desorption process without limitation by the electrochemical kinetics, eventually lead to form electrical double layer capacitance as depicted in Fig. 1. Thus, the specific capacitance (C_{sp}) is described to evaluate the charge storage ability of SCs [24]:

$$C_{sp} = \frac{\Delta Q}{\Delta V \varepsilon} = \frac{I \Delta t}{\Delta V \varepsilon} \quad (1)$$

The specific capacitance C_{sp} of SCs is a reflection of the electrical charge ΔQ stored at a voltage change ΔV, where ε refers to the mass, surface area or volume of the electrode materials. Hence, C_{sp} is often corresponding with the gravimetric capacitance (F g^{-1}), areal capacitance (F cm^{-2}), and volume capacitance (F cm^{-3}). Besides, C_{sp} can be utilized to assess device performance, when normalized by the weight or volume of the whole device.

Additionally, EDLCs with absence of faradic redox reactions also prevent the swelling of active materials emerging in the process of charge/discharge cycles. Hence, EDLCs have capacity in sustaining millions of cycles whereas batteries have a few thousands at most. However, the restriction of the charge at the electrode surface causes the lower energy density compared with rechargeable batteries. Because the value of energy density (E) accumulated in a capacitor is related to the C_{sp} and operating voltage (V_0) according to formula 2 [15]:

$$E = {}^1\!/\!_2 C_{sp} V_0 \quad (2)$$

While the maximum power density is depicted as [11]:

$$P = \frac{V_0^2}{4 R_{ESR} \varepsilon} \quad (3)$$

where R_{ESR} represents the equivalent series resistance (ESR). The energy storage capacity of SCs can be promoted by improving the specific capacitance or the cell voltage. It is a useful method to enhance the specific capacitance by introducing pseudo-

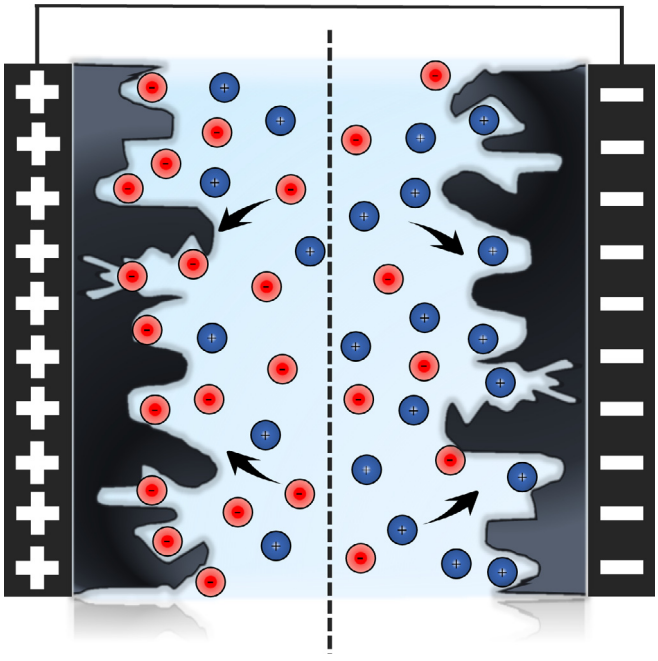

Fig. 1. Schematic of EDLCs charge storage mechanism at electrodes.

capacitance from the surface reactions. It is also necessary to develop materials with high electrical conductivity since R_{ESR} is closely related to the resistance of the electrode materials themselves.

Based on fast reversible redox reactions happened on the thin surface layer (tens of nanometer) of active materials, the charges are faradically stored in pseudo-capacitors. Generally, the capacitance of PCs is higher than EDLCs, but the cycling lifespan of PCs is relatively poor [5,25].

1.2. Carbon materials for supercapacitors

In the past, various classes of carbon materials, such as graphene (GN), active carbon (AC), carbon nanotubes (CNTs), carbon nanofibers (CNFs), carbon onion, etc. [3,26–30], have been in-depth studied for EDLC electrodes. Owing to the high SSA, abundant porosity and good electrical conductivity, carbon materials possess the advantages in power performance and cycling stability [31–37].

As a result of the environmental friendliness, inexpensive and abundance in nature, renewable resource based materials have been widely used in fabrication of SCs electrodes corresponding with the sustainable development. These kinds of biomaterials could be easily found in daily lives, such as parts of the plant (shaddock peel, bamboo, petals, etc.), raw materials from animals (silk, crab shell, honeycomb, etc.) and primary metabolism products like cellulose and starch as shown in Fig. 2 [25,38–46]. Particularly, tremendous scientific studies have been made on the subject of using cellulose, bacterial cellulose (BC), and lignin to manufacture biomass-based electrode materials [47–51]. BC, consisting of random orientational nanofibers and plentiful surface hydroxyl groups, has the three-dimensional (3D) porous interconnected nanofibrous network and outstanding tensile strength (>2 GPa) [52]. On account of their great hydrophilicity, BC also favors in the diffusion of aqueous electrolyte. Lignin is an abundant and economical by-product of pulping and paper industries. Unlike cellulose composed of single monomeric linkages, lignin has no regular structure within its polymeric framework. It has been widely studied for its abundance as a typical polymer among a good many nature resources [53–55], and the development of lignin may bring about the prosperity of wood-to-ethanol bio-refineries in future [56]. The resulting electrode materials prepared by reported procedures and their application for the related energy generation, storage, and conservation fields, are regarded as a promising model of green chemistry, sustainable development and biomass valorization.

1.3. How to improve the specific capacitance performance of carbon materials

1.3.1. Tuning the porous structure

Micropore (<2 nm), mesopore (2–50 nm) and macropore (>50 nm) classified from IUPAC are employed to describe the pore size [57,58]. The average pore size, pore size distribution (PSD), SSA and pore volume are the most significant parameters for the adsorption of charged ions. Furthermore, amounts of researches have shown that the EDLCs from carbon materials are closely related to the electrolyte accessibility of electrode surface. It should be noted that effective SSA (E-SSA) also has important impacts on capacitance performance of carbon materials. Different from the total SSA calculated from the Brunauer-Emmett-Teller (BET) model, E-SSA is controlled by both the total SSA, PSD of the electrode materials and the size of electrolyte ion [59–61]. It indicates that carbon electrode materials with porous structure, high E-SSA and optimal PSD, maintain higher capacitance at relatively high current density [11,56,62–65].

As previous studies demonstrate that the micropores and channels are most effective in a process of double-layer formation, while may slow down the kinetics of ion transportation to some extent [66]. Mesopores reduce resistance of ion diffusion and macropores help to form ion buffering reservoirs to decrease the ion transportation distance after electrolyte penetration. Large amounts of combinations of different PSDs and various scale of porosity have also been studied. The synergistic effects of hierarchically porous structure ensure high affinity of charge transfer and faster ion diffusion process. Hence, the constructions of hierarchical electrodes enable unimpeded ion transportation and good capacitance of SCs. Detailly, the interconnected mesopores render low-resistance pathways for the ions diffusion at the inner-pore surface, and the large space of macropores can strengthen the possible electrostatic adsorption area to enhance the rate capability of SCs. Besides, the hierarchically macroporous and mesoporous combinations not only promote the free access of ion to the in/exterior surface of materials and shuttle across the channels, which is favorable for electrolyte penetration and electrochemical reactions, but also provide a large SSA for high mass loading of the electroactive materials [67,68]. It should be noted that charges store in suitable nanopores which are propitious to confine themselves [69]. Additionally, a universal theoretical model illustrates the charge storage mechanism correlations with pore size and distributions [70,71]. It appears that (de)-solvated ions form electric wire-in-cylinder capacitor in the micropores, while have conformations of electric double-cylinder capacitor near the pore wall in the mesopores. However, this model is only applicable for carbon materials with unimodal pores, not suitable for PCs. Such above-mentioned carbon materials with developed porosity could possess optimized energy storage capabilities and excellent cycling stability. Therefore, strategies to synthesize the porous materials are crucial to maximize electrochemical performance of SCs. In addition, many micro/nanoscale materials become the mainstream of electrode materials for their unique characteristics in mechanical performance, electrical and thermal conductivity [5,9,32,72].

1.3.2. Physical and chemical activation

As a key parameter in assessing morphology of carbon materials, porosity has great effects on the surface area of resulting products. In order to achieve higher performance, physical and chemical activation have been taken to obtain abundant porous structure.

The physical activation method is commonly occurred with carbon dioxide or water steam at high temperature (800–1000 °C), and forms abundant porous structures on the surface and inside of the carbon bulk materials as described in equations below [56]:

$$C + CO_2 \rightarrow 2CO \quad (4)$$

$$C + H_2O \rightarrow CO + H_2 \quad (5)$$

Porosity in AC is determined by the activation methods and the precursor materials. The activation reaction achieves the purpose of pore formation through the following three steps [73]. Initially, open of previously inaccessible pores which are blocked by disordered carbon atoms and heteroatoms. In the second step, the carbon of the elementary crystals reacts with oxidative gas at the surface to form gaseous oxides. In the last stage, the existing micropores are continuously enlarged, and walls between adjacent micropores completely collapse to form larger pores [74–78].

The other method, chemical activation simultaneously proceeds with carbonization steps at a relatively low temperature under the protection of an inert gas. Porous structure could be obtained after heat treatment of the mixture of carbon materials and the

activation reagents such as KOH, NaOH, $ZnCl_2$, NH_3, $NaNO_3$, etc. [79–83] For instance, chemical activation mechanism of carbon materials with KOH or K_2CO_3 is suggested as [84,85]:

$$6KOH + 2C \rightarrow 2K + 3H_2\uparrow + 2K_2CO_3 \quad (6)$$

$$K_2CO_3 + 2C \rightarrow 2K + 3CO\uparrow \quad (7)$$

The microstructural evolution is as depicted in (6) and (7). K_2CO_3 is first produced during the activation process at high temperature. The subsequent reaction eliminates carbon atoms and leaves behind numerous vacancies on the materials, in which the following removal of K_2CO_3-occupied and K-bound sites results in micropores [86].

Zinc chloride works effectively as dehydration reagent below 600 °C. Firstly, it transforms into hydrated zinc chloride ($ZnCl_2 \cdot nH_2O$). In the following stabilization, $ZnCl_2 \cdot nH_2O$ seems to hydrolyze and generate an oxychloride [87]:

$$ZnCl_2 + 1/2\ O_2 \rightarrow ZnOCl + 1/2\ Cl_2 \quad (8)$$

$$2ZnO + C \rightarrow 2Zn + CO_2\uparrow \quad (9)$$

Zinc oxide decomposes from the oxychloride in thermal process. Then ZnO facilitates to produce micropores on the outer surface of materials by etching carbon atom. Similarly, NH_3 as activated agent reacts with the carbon material to produce volatile gas. The decomposition of the carbon structure through the gasification reactions is described below [88]:

$$C + NH_3 \rightarrow HCN + H_2 \quad (10)$$

$$C + 2H_2 \rightarrow CH_4 \quad (11)$$

The carbon structure is collapsed and micropores are generated simultaneously. Hence, the carbon precursor converts into activated carbon with disordered carbon phase.

As to $NaNO_3$, it has good water solubility, decomposability and expansibility in high temperature. Besides, $NaNO_3$ not only serves as a nano-confine hard template for creating macropores (50–150 nm), but also acts as a activation reagent to generate mesopores (2–4 nm) [89]. $NaNO_3$ template could be easily removed via water washing leaving no residue. The formation of mesopores above 600 °C undergoes a mechanism as the following equations:

$$12NaNO_3 \rightarrow 6Na_2O + N_2\uparrow + 10O_2\uparrow + 10NO\uparrow \quad (12)$$

$$2Na_2O + C \rightarrow 4Na + CO_2\uparrow \quad (13)$$

Firstly, this in-situ etching treatments of Na_2O and CO_2 create abundant micropores. Then, the expansion movement of the released gases (N_2, O_2, NO) can enlarge the pore size.

As oxygen groups are always exhibited on the surface of carbon materials after activation and carbonization processes, pseudo-capacitive contribution should be considered [22]. It has been reported that low capacitance (around 50–80 $F\,g^{-1}$) of untreated CNTs or CNFs could be reached more than 100 $F\,g^{-1}$ through introducing oxygen-rich groups. However, this oxygen-containing groups are harmful to cycling stability of SCs [23,38,90,91]. The carbonaceous materials of EDLCs are generally pre-treated before fabrications so as to remove moisture and excess functional groups on the materials surface [92–94]. These oxygen-containing functional groups are classified into three kinds of types: phenol group (C–OH), quinone oxygen group (C=O) or ether group (C–O–C), and carboxylic group (COOH) [95]. The reactions of pseudo-capacitance for different functionalized oxide groups are present as follow [96]:

$$C{-}OH \Leftrightarrow {>}C{=}O + H^+ + e^- \quad (14)$$

$$-COOH \Leftrightarrow -COO- + H^+ + e^- \quad (15)$$

$${>}C{=}O + e^- \Leftrightarrow {>}C{-}O^- \quad (16)$$

The reaction (14) and (15) only represent a quasi-reversible or irreversible character in the basic electrolyte, while contribution of pseudo-capacitance is mainly derived from the reaction (16) taking place at the electrode interface, in which the carbonyl groups store and release an electron without ion exchanges.

In contrast to the physical activation, chemical activation has the advantages of short activation time, easy control of activation reaction, etc. However, chemical activation may introduce excessive functional groups which lower the electronic conductivity and may be harmful to the rate capability and stability. In some cases, chemical activation may result in uncontrollable PSD. After activation processes, the surface chemical/physical properties of activated materials still maintain balanced. Simultaneously, EDLCs based materials possess high SSA, innovative nano-structures, controllable PSD and enhanced surface wettability, which promote accommodation of ions and facilitate formation of electrical double layer and partial pseudo-capacitance.

1.3.3. Heteroatom doping

Heteroatom doping has been regarded as one of the most effective ways to enhance the wettability of carbon materials and introduce pseudo-capacitance. It has been reported that mono, dual, and even tri-heteroatom (N, B, P, S, F, Cl, Si, etc.) doping have been adopted to strengthen the electrochemical activity by adjusting the inherent properties of materials such as band gap. Owing to defects in the C atoms, the electro-neutrality of the carbonaceous materials is deviated. These defects generated by heteroatom doping also promote some redox reactions and make carbon materials become catalytically active [97–101].

Heteroatoms can significantly enhance the hydrophilicity and polarity of carbonaceous material, thus enlarge the electroactive surface areas, electronic conductivity, charge densities of carbon atoms and result in high electron donating property. It could be concluded that the inherent hydrophobicity of certain carbonaceous materials prevents the penetration of electrolyte solutions and hinders improvement of the capacitive performance of SCs devices. After heteroatoms doping treatments, the surface chemical/physical characteristics of these materials can be modified, and more electro active sites have been offered that are beneficial to charges storage. Among several types of heteroatom doping, nitrogen-doping has been widely researched by using N-containing precursors, such as melamine, polyaniline, polyacrylonitrile, etc., or post-treatment of porous carbon materials with amines and urea to introduce N-rich groups on the surface of materials [102]. The nitrogen species are usually divided into four different types: pyridinic nitrogen (N-6), pyrrolic/pyridone nitrogen (N-5), quaternary nitrogen (N-Q) and pyridine-N-oxide (N-X). Pseudo-capacitance is introduced via positively charged N-Q and N-X, which promote electron transfer through carbons and also by negatively charged N-5, N-6 [103–106]. Among these four doping types, pyridinic and pyrrolic nitrogen are considered as two important factors contributing to pseudo-capacitance due to their originating from defects in carbon. It has been shown that urea prefers to form N-6 species, but melamine have tendency to form N-Q. That is because of the different chemistries of the N-sources [107]. The mechanism of N-

doped pseudo-capacitance is depicted as the following electrochemical reactions on the carbon surface [102]:

$$C^{*}\text{- } NH_2 + 2OH^{-} \leftrightarrow C\text{ - }NHOH + H_2O + 2e^{-} \quad (17)$$

$$C^{*}H\text{ - } NH_2 + 2OH^{-} \leftrightarrow C + NH + 2H_2O + 2e^{-} \quad (18)$$

Where C* stands for the carbon network. The redox mechanism of nitrogen dopants is believed to attract protons and improve the charge density of space charge layer.

Boron atoms in a carbon lattice can facilitate the chemical adsorption of oxygen to form a carbon surface with reactive activity [108,109]. It is thus a highly promising candidate for doping of carbon materials as illustrated in eqn (19) [110]:

$$xB_2O_3 + (2 + 3x)C \rightarrow 2B_xC + 3xCO\uparrow \quad (19)$$

B_2O_3 starts to be melting and then vaporizes with reaction temperature rising. After removing oxygen groups, active sites are provided for boron doping into carbon matrix.

Phosphorus atoms have the ability in stabilizing oxygen functional groups during charging, thereby improving the stability and selectivity of redox-reactions. The faradaic redox reactions in acid and alkaline electrolytes are illustrated in the following formulas [111]:

$$-P{=}O + 2e^{-} + 2H^{+} \Leftrightarrow -PH{-}OH \quad (20)$$

$$-P{=}O + 2e^{-} + 2H_2O \Leftrightarrow -PH{-}OH + 2OH^{-} \quad (21)$$

$$-PH{-}OH + 2e^{-} + 2H^{+} \Leftrightarrow -PH_2 + 2H_2O \quad (22)$$

Sulfur-containing functional groups are reported to decrease the shrinkage of micropores during the carbonization step and support the larger pores at high temperatures, which provide fast ion transportation without causing unnecessary redox reactions. The sulfur species contribute to pseudo-capacitance by the reactions as presented [112]:

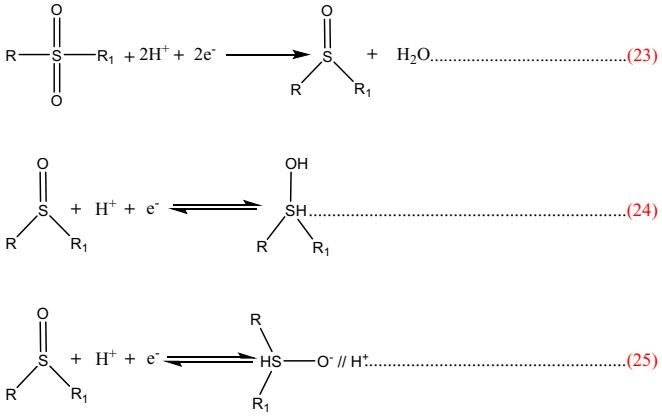

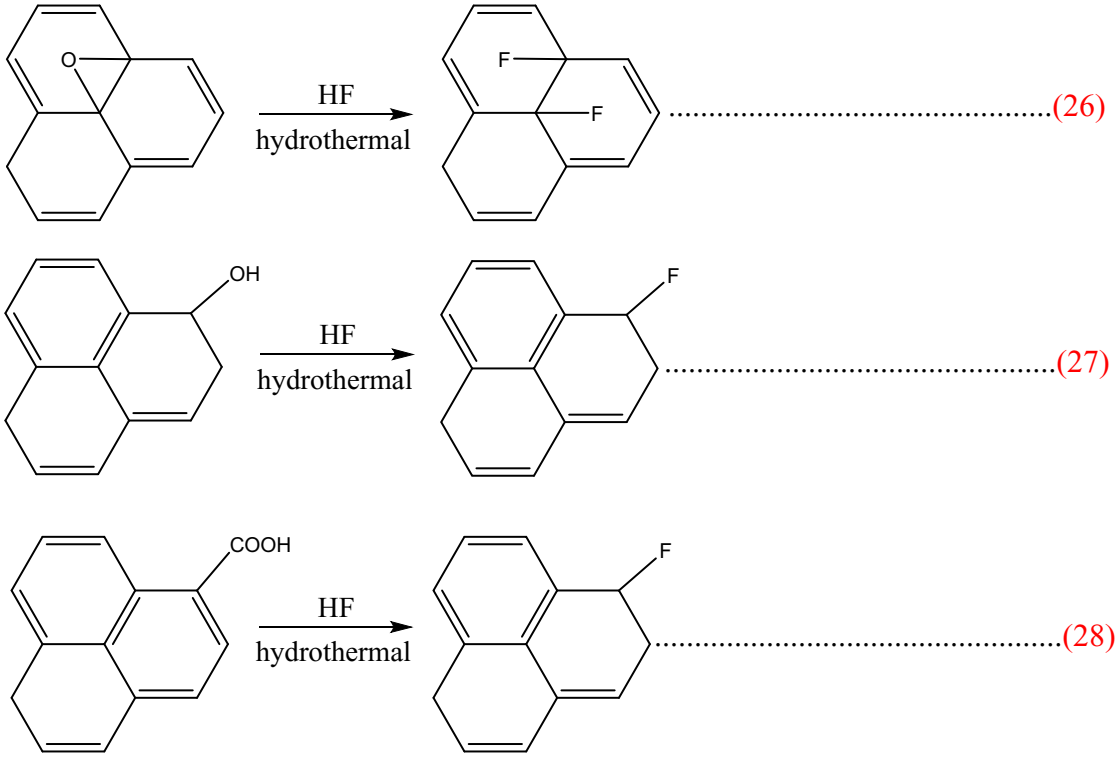

Firstly, parts of sulphone-groups are reduced into sulfoxide-groups (23). Then, sulfoxide-groups are further transformed into sulfenic acid (24). Some of sulfenic acid become ionized and have adsorption of H^{+} (25).

In particular, introduction of fluorine is an effective approach to optimize the conductivity of carbon electrodes due to the synergistic effects of increasing disorder and defects. Those can expand interlayer spacing and create numerous active sites of semi-ionic C–F bonds [113,114]. Fluorination enhances polarization from the highly electronegative fluorine functional groups and the refinement of pore structures/surfaces in non-aqueous electrolytes. It is proposed that there are three substitution reactions involving

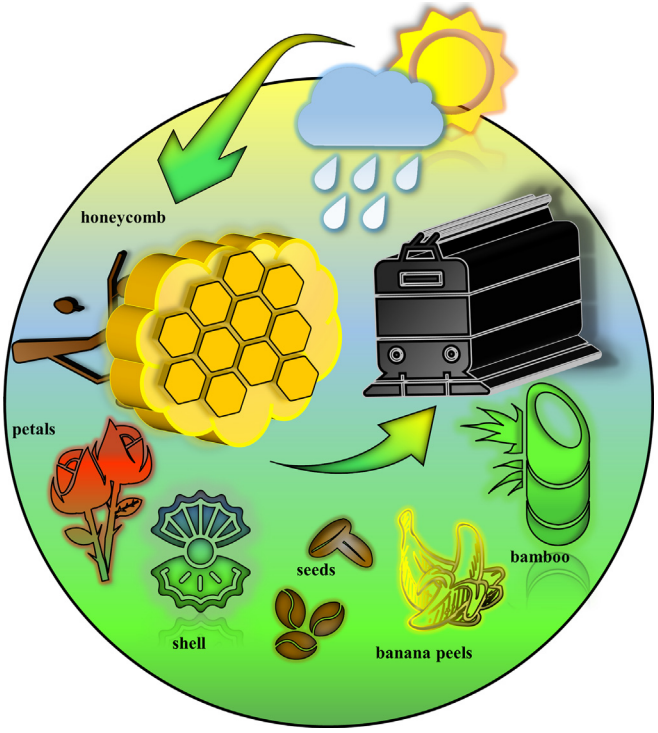

Fig. 2. Schematic of biomass-derived carbon precursors. (A colour version of this figure can be viewed online.)

fluorine atoms during the hydrothermal process, as shown in equations [115]:

In addition to mono-heteroatom doping, dual and tri-doping have also been applied in SCs due to their synergistic effects. N/B co-doped GN aerogels were obtained for all-solid-state supercapacitors. Electrochemical tests have indicated the highest capacitances of over 60 F g^{-1} for the dual-doped samples [116]. As presented by Yang and co-workers, the N/Si/P-doped CNF showed the synergistic effect on surface wettability of the electrodes. Among these three elements, phosphorus and silicon groups facilitate the formation of EDLC, as well as nitrogen enhances the pseudo-capacitance effect [117].

2. Design binder-free carbon materials for supercapacitors

2.1. Why design binder-free structures

Flexible wearable electronic devices such as artificial electronic skin, bendable display, e-textile and so forth [10,118–124], have caught the mainstream of developing portable electronic. In order to fabricate the lightweight and flexible SCs, large numbers of researchers focus on manufacturing free-standing electrode materials. However, the ultimate products are difficult to be self–supported for most of nature resources, which implies that additives with death mass are needed for guaranteeing a high conductivity [125,126]. In typical designs of SCs, there are many parameters and metrics should be considered (Fig. 3). Among them, additives of binders such as poly (tetra fluoroethylene) (PTFE), poly (vinylidene fluoride) (PVDF) and conductive agents of carbon black (CB), acetylene black (AB) are the common adding components of electrode materials. Those additives are used to enhance the electric contact between current collector and electroactive materials to reduce the electrical resistance of electrodes. But, the side effects of those additives cannot be ignored. It is inevitable to increase the total weight of the device (taking about 10–20%) and cost of production. The addition of additives also weakens the electrochemical performance of SCs such as specific capacitance, energy and power density [127]. Aroused by aforementioned drawbacks, binder-free carbon materials have been prepared, which favor rapid mass/charge transport and bring about abundant accessible active sites without compromising the volumetric performance and commercial values. It has been reported that the CNTs without binders were fabricated via vacuum filtration and chemical vapor deposition (CVD) methods [128,129]. Owing to their robust mechanical property and excellent conductivity, these CNTs could be directly employed as electrode materials for SCs. Besides, these electrode materials typically deliver a high power density more than 100 kW kg^{-1}. Hence, it is necessary to use binder-free structural electrodes to achieve higher electrical conductivity, specific capacitance, better cycling and mechanical stability at high current densities.

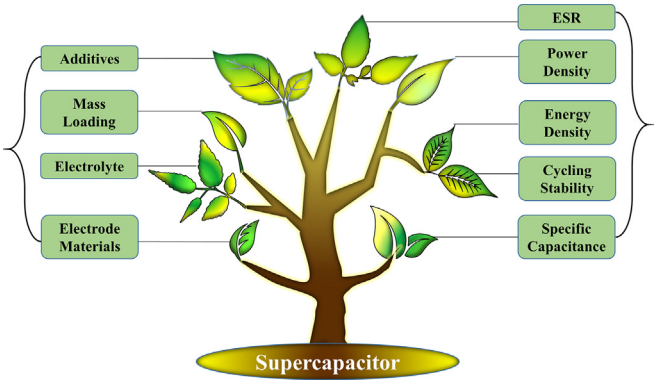

Fig. 3. An illustration of key performance metrics and major affecting factors for SCs.

2.2. How to obtain binder-free carbon material

In order to assemble self-supported electrode materials, extended studies have been done from materials themselves and fabrication technologies to construct the structural electrode materials. There are mainly two approaches for fabricating free-standing electrode materials, “bottom-up” and “top-down” [35,130]. According to the former method, small building blocks of carbon resources including CB, CNTs and GN, are built into free-standing structures through filtration, hydro-thermal assembling, electrospray-deposition, wet spinning, etc. [131–140] In the latter way, self-supported carbon precursors (CNFs mats, carbon cloth, paper, etc.) can serve as substrates to load electroactive materials [141–143]. “Top-down” methods are commonly used and convenient because of the cost-efficient substrates and simple fabricating processes [144].

2.2.1. Carbonization of paper and cloth

As mentioned before, carbon materials based on EDLCs have been widely studied to manufacture electrode materials with different morphologies via carbonization treatments. Owing to the abundance of biomass, it is reasonable for industry to achieve large-scale productions. At the lab scale, researchers generally carbonize the biomass precursors under high temperature (700–1000 °C) protected by inert gas to get carbon paper, carbon cloth, carbon fabric, and their solid derivatives (Fig. 4) [67,121]. Those carbonized products with unique structures have advantages in charge transfer and provide a fast access for electrolyte ion into the surface of electrodes.

2.2.2. Pyrolysis of precursors with gel or monolith structure

The conventional carbon powder materials have limited

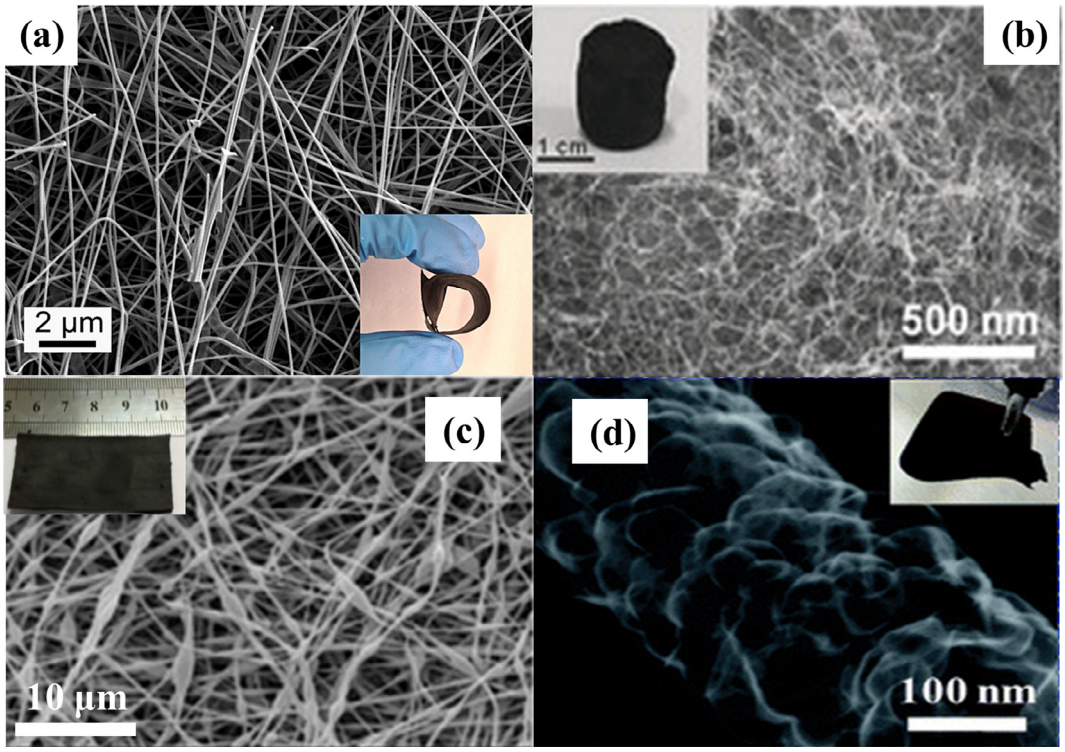

Fig. 4. Different carbonaceous materials after carbonization: (a) Lignin/polyvinyl alcohol (PVA) composite nanofiber mats [145]. (b) Wood-derived CNF aerogels [146]. (c) Lignin-based electrospun carbon fibers [147]. (d) Electrospun flexible carbon nanofiber webs [148]. The insets depict the corresponding optical photos. (A colour version of this figure can be viewed online.)

utilizations owing to their dusting and complicated electrode operation steps. Hence, the carbon monolith or carbon aerogels are applied to settle these above problems [149]. Carbon monolith with free-stranding 3D structure, exhibits the advantages in desirable microstructure, high electrical conductivity of 10^3–10^6 S cm^{-1}, easy shape processing and mechanical stability. Unlike other powdered carbon materials, carbon monolith can be directly utilized as thick electrode for SCs without adding inactive additives. Meanwhile, 3D porous carbon monolith with high SSA strengthens mass transfer kinetics, charge storage, and electrolyte accessibility [128,150]. The porous carbon monolith is often synthesized through template methods. Soft template (F127, P123, etc.) and hard template (mesoporous silica, KIT-6 and soluble salts) [151] are used in the preparation. During the fabrication processes, a freeze-drying treatment enables a surface coating with carbon sources, and they are further transformed into carbon scaffold during pyrolysis at high temperature. After removal of the templates, the monolith has been successfully obtained [152,153].

Considering the unique structure of carbon aerogel, it has fascinating properties of ultralight, high electrical and thermal conductivity, abundant continuous porosity, large SSA and chemical stability [154–156]. Carbon aerogels are regarded as suitable supporting materials for anchoring of electroactive materials or directly used as electrodes. Based on the carbon resources, carbon aerogels can be divided into three categories, including carbon-based (graphene, CNTs, etc.), synthetic organic polymer-based, and biomass-based (BC, wood, cattail, etc.) [157]. The traditional synthetic route of carbon aerogel materials includes a sol–gel method that replaces the liquid solvent in gels via air or template-assisted synthesis. Upon pyrolysis processes protected by inert gas at high temperature, the cross-linked aerogels are transformed into carbon aerogels [158,159]. The carbon aerogels with 3D nanoscale interconnected porous networks provide low-resistance pathways for ions transportation and good rate performance, which holds great potential for binder-free energy-storage devices. But the electrochemical performance of SCs is often hindered by their intrinsic hydrophobicity, structure-derived fatigue failure and weak elasticity [160,161].

2.2.3. Electrospinning to make nanofiber films/mats

Electrospinning is a facile and continuous approach to produce ultrathin fibers (sub-micrometer to few nanometers) [162–167]. Electrospinning consists of an electro-hydrodynamic process, in which the droplet of polymetric solution or melt is electrified to generate a liquid jet under a high electric field, subsequently undergoes the processes of stretching and elongation [168–172]. After stabilization in air and carbonization at inert atmosphere, the as-spun nanofibers can be converted to carbon nanofiber film with uniform diameters. The fabrication of electrospun fibers and their dimensions could be controlled by the processing parameters of viscosity polymer solution, applied voltage, feeding rate, collector distance, humidity, temperature, etc. [8,145,173–175] Electrospun nanofibers have their intrinsic high porosity, large surface to volume ratios and excellent stability against corrosive electrolyte supposed as ideal materials in energy harvest fields. Porosity can be generated via adding of salts and phase separation. Furthermore, the electrospun fibers with designed architectures of nanobelts, core–sheath, multichannel microtubes and hollow nanotubes, have been realized through electrospinning technique [147,176–182]. Hence, the electrospun nanofiber electrode delivers the desirable features such as large electrode interface, rapid electrons/ions transfer and enhanced electrochemical properties, making them attractive for binder-free and wearable electronic devices [72,183].

2.2.4. Filtration carbon particles to make films/membranes

Vacuum filtration is a continuously facile physical filtration technique used to separate solids from liquids without requirement

Table 1
Preparation of biomass derived carbon materials for free-standing electrodes and their electrochemical performance.

Biomass Resource	Preparation Method	Electrode Material	S_{BET} ($m^2\ g^{-1}$)	V_t ($cm^3\ g^{-1}$)	V_{micro} ($cm^3\ g^{-1}$)	Average diameter of pores (nm)	C_s ($F\ g^{-1}$)	E_{max} ($Wh\ kg^{-1}$)	W_{max} ($kW\ kg^{-1}$)	Ref
Cotton	800 °C 2 h, $m_{(C)}$:$m_{(KOH)}$ = 1:3 at 700 °C 2 h	Carbon/GN cloth (N: 3.1%)	1284	0.62	0.51	1.9	92 $F\ g^{-1}$ at 0.1 $A\ g^{-1}$ in 6 M KOH	11.4 $Wh\ L^{-1}$	3.2 $kW\ L^{-1}$	[191]
	900 °C 2 h, $m_{(C)}$:$m_{(KOH)}$ = 1:2 at 800 °C 2 h	AC-rGO films	392.6	0.25	0.15	0.50	120 $F\ g^{-1}$ at 3 $A\ g^{-1}$ in PVA/KOH	240 $\mu Wh\ cm^{-2}$	156 $mW\ cm^{-2}$	[192]
	800 °C 2 h, $m_{(C)}$:$m_{(NaOH/urea)}$ = 0.75:1	CFs	584.5	0.39		2.6	221.7 $F\ g^{-1}$ at 0.3 $A\ g^{-1}$ in 3 M KOH			[193]
	800 °C 1.5 h, $m_{(C)}$:$m_{(KOH)}$ = 1:6 at 800 °C 1.5 h	Carbon fiber aerogel	2307	1.18	0.77	2.0	224 $F\ g^{-1}$ at 100 $A\ g^{-1}$ in 6 M KOH			[84]
	950 °C in N_2	Carbon fiber aerogel (N: 1.97%)	2183	1.83	0.09	11.2	327.7 $F\ g^{-1}$ at 0.2 $A\ g^{-1}$ in 6 M KOH	16.1	3.7	[194]
	800 °C 2 h in N_2	Carbon nanoprism/CC (N: 10.4%)	50.4	0.05		4.0	38.8 $mF\ cm^{-2}$ at 0.5 $mA\ cm^{-2}$ in 6 M KOH			[195]
	800 °C 1 h in Ar and NH_3 ($V_{(Ar)}$:$V_{(NH3)}$ = 100:65)	*Cc* (N: 9.6%)	1085			0.5–2	207 $F\ g^{-1}$ at 1 $A\ g^{-1}$ in 1 M H_2SO_4	7.2	3.83	[196]
	800 °C 1 h in N_2	rGO carbon aerogel (N: 1.77%)	728.6	0.66	0.31	3.5	270 $F\ g^{-1}$ at 0.1 $A\ g^{-1}$ in KOH/PVA	29	2.24	[197]
	800 °C 1 h in Ar and H_2 ($V_{(Ar)}$:$V_{(H2)}$ = 40:3)	CNTs/Cc	136.5			3.6	1.14 $F\ cm^{-2}$ at 2.5 $mA\ cm^{-2}$ in PVA/H_2SO_4	1.6 $mWh\ cm^{-3}$	75.3 $mW\ cm^{-3}$	[198]
	800 °C 1 h, $m_{(C)}$:$m_{(urea)}$ = 1:4 in N_2	GN aerogel/Cc (N: 3.5%)	398.9	0.24	0.09	3.7	200 $F\ g^{-1}$ at 0.1 $A\ g^{-1}$ in PVA/KOH	20	4	[199]
Bacterial cellulose	800 °C 3 h in N_2	CNFs	624	0.67		4.3	184 $F\ g^{-1}$ at 0.25 $A\ g^{-1}$ in 6 M KOH	6.9	5.82	[200]
	900 °C 1 h in Ar	rGO/CNFs	137				216 $F\ g^{-1}$ at 0.1 $A\ g^{-1}$ in 6 M KOH			[201]
	600 °C 2 h, $V_{(CO2)}$/$V_{(Ar)}$ = 0.5% at 800 °C 0.5 h	CNFs (N: 9.44%)	312.5	1.07		13.7	150.3 $F\ g^{-1}$ at 100 $A\ g^{-1}$ in 2 M H_2SO_4	6	390.53	[202]
Silk	900 °C 2 h in N_2	Carbon microfibers (N: 4.52%)	230			6	189 $F\ g^{-1}$ at 0.5 $A\ g^{-1}$ in 6 M KOH			[203]
	600 °C 2 h in N_2	Carbon microfiber (N: 10.9%)	115			1.6–4	225 $mF\ cm^{-2}$ in PVA/H_2SO_4	22.7 $\mu Wh\ cm^{-2}$	10.26 $mW\ cm^{-2}$	[204]
	900 °C 2 h in N_2	Carbonized silk fabric (N:4.4%)	256.6	0.03		2.02	255.9 $F\ g^{-1}$ in 1 M Na_2SO_4			[205]
	900 °C 2 h in N_2	Carbonized silk fabric (N:6.6%)	285.1	0.027		1.97	305 $F\ g^{-1}$ in 1 M Na_2SO_4	10.73	1.21	[206]
	700 °C 2 h in N_2	AC (N:3.35%)	499	0.24			48.6 $F\ g^{-1}$ at 0.7 $mA\ cm^{-2}$ in PVA/Na_2SO_4	17.2	0.21	[207]
	600 °C 2 h, $m_{(C)}$:$m_{(KOH)}$ = 1:4 at 800 °C 2 h	Graphitic AC (N: 1.9%)	1927	0.83		3.19	52.8 $F\ g^{-1}$ at 0.18 $A\ g^{-1}$ in 6 M KOH	7.4	0.9	[208]
Lignin	900 °C under 1 v% O_2 in N_2	Submicron CFs	1005	0.44		1.2–1.7	45 $F\ g^{-1}$ at 1 $A\ g^{-1}$ in 1 M Na_2SO_4	5	61	[209]
	850 °C 0.5 h in N_2	Submicron AC fibers					344 $F\ g^{-1}$ in 6 M KOH	8.1	2.98	[190]
	750 °C 1 h, $m_{(C)}$:$m_{(KOH)}$ = 1:4 in N_2	GO/lignin carbon films	1744	0.816	0.67		165 $F\ g^{-1}$ at 20 $A\ g^{-1}$ in 1 M H_2SO_4	5.6	2.5	[210]
	900 °C 0.5 h in N_2, and 800 °C 1 h in CO_2	CFs	1204	0.55		0.39	155 $F\ g^{-1}$ at 0.1 $A\ g^{-1}$ in 6 M KOH	0.6 $mWh\ cm^{-3}$	10.6 $W\ cm^{-3}$	[211]
	800 °C under 5% H_2 in N_2	CNFs	1249	0.52	0.44		192 $F\ g^{-1}$ at 0.1 $A\ g^{-1}$ in 6 M KOH	2.25 $mWh\ cm^{-3}$	10.3 $W\ cm^{-3}$	[212]
	1000 °C 1 h in He, and 800 °C 0.5 h in CO_2 and N_2 (1:4)	CNFs	2170	0.99	0.62		87 $F\ g^{-1}$ at $Pyr_{14}TFSI$ (mixed with PC and EC)	38	1.67	[213]
	1200 °C 1 h in Ar	CNFs	583	0.29		3.5	64 $F\ g^{-1}$ at 0.4 $A\ g^{-1}$ in 6 M KOH			[145]
	900 °C 0.25 h in Ar	Carbon monolith	803	0.86			2.2 $F\ cm^{-2}$ in 6 M KOH	0.16 $mWh\ cm^{-2}$	309.5 $mW\ cm^{-2}$	[214]
Cellulose acetate	800 °C 1 h in Ar	CFs	1173	0.41	0.32	1.9	280 $F\ g^{-1}$ at 0.1 $A\ g^{-1}$ in 6 M KOH			[215]
	700 °C 1 h in N_2 (20% $ZnCl_2$)	Electrospun CNFs	1188	0.58	0.41	1.9	202 $F\ g^{-1}$ at 0.1 $A\ g^{-1}$ in 6 M KOH			[216]
Starch	650 °C 2 h, $m_{(C)}$:$m_{(KOH)}$ = 1:2	AC/CC	1367.9	0.57		0.60	272 $F\ g^{-1}$ at 1 $A\ g^{-1}$ in 6 M KOH	25.9	11.3	[217]
	1400 °C 1 h under vacuum	CNTs/CNFs	350	0.31		4.6	170 $F\ g^{-1}$ in 1 M H_2SO_4			[218]
Sucrose	650 °C 2 h, in Ar and H_2 ($V_{(Ar)}$:$V_{(H2)}$ = 1:1)	Carbon monolith	770	2.0	0.24	18	75 $F\ g^{-1}$ in EMITFSI			[152]
	1400 °C 3 h in Ar	GN membrane	710	0.8			190 $F\ g^{-1}$ at 1 $A\ g^{-1}$ in 1 M $TEABF_4$/AN	50	340	[219]
	700 °C 2 h in vacuum, 900 °C 2 h under CO_2	AC	1636	0.79	0.52		325 $F\ g^{-1}$ at 4.5 $A\ g^{-1}$ in 1 M H_2SO_4			[220]
	800 °C 3 h in Ar	Carbon monolith	705	0.32	0.30	0.6	200 $F\ g^{-1}$ at 0.2 $A\ g^{-1}$ in 2 M H_2SO_4	15	1.59	[221]
	900 °C 2 h in N_2	Carbon microfibers (N: 4.2%, K: 6.2%)	578.3	0.27		0.57	172 $F\ g^{-1}$ at 1 $A\ g^{-1}$ in 1.5 M $TEABF_4$/ACN	53.7	15.8	[222]
Chitosan	800 °C 2 h in N_2	Carbon aerogel (N: 5.47%)	554		0.25		261 $F\ g^{-1}$ at 0.5 $A\ g^{-1}$ in 1 M H_2SO_4			[223]
Bamboo	800 °C 2 h in Ar	Carbon/GN aerogel (N: 6.22%)	487				225 $F\ g^{-1}$ at 0.25A g^{-1} in 2 M H_2SO_4	31.3	12.9	[224]

(*continued on next page*)

Table 1 (*continued*)

Biomass Resource	Preparation Method	Electrode Material	S_{BET} ($m^2 g^{-1}$)	V_t ($cm^3 g^{-1}$)	V_{micro} ($cm^3 g^{-1}$)	Average diameter of pores (nm)	C_s ($F g^{-1}$)	E_{max} (Wh kg^{-1})	W_{max} (kW kg^{-1})	Ref
Basewood	950 °C 2 h, activation at 950 °C 0.5 h in NH_3	Wood carbons (N: 5.2%, S: 0.3%)	1438	1.36	0.40	3.2	135 $F g^{-1}$ at 0.2 $A g^{-1}$ in 4 M KOH	15.2	3.23	[225]
Gelatin	900 °C 2 h in Ar	Carbon film (N: 7.4%)	60.8			30	168 $F g^{-1}$ at 5 $A g^{-1}$ in 2 M Na_2SO_4			[226]
Peanut shell	800 °C 2 h, $m_{(C)}$:$m_{(KOH)}$ = 1:3 at 800 °C 2 h	AC	2070	1.33		1.3	186 $F g^{-1}$ at 0.5 $A g^{-1}$ in 1 M H_2SO_4	58.3	37.5	[227]
Chitin	900 °C 6 h in N_2	Carbon nanorods (N: 4.6%)	1000	0.88		4	138 $F g^{-1}$ at 0.92 $A g^{-1}$ in 1 M H_2SO_4			[228]
Sisal leaves	1000 °C in Ar	AC	1137	1.37		0.40	204 $F g^{-1}$ at 1 $A g^{-1}$ in 1 M LiOH			[229]
Viscose cloth	630 °C 2 h in N_2, 930 °C 1 h under CO_2	AC cloth	1205	0.47	0.46	0.78	121 $F g^{-1}$ at 0.02 $A g^{-1}$ in 1 M H_2SO_4			[230]

S_{BET}: BET of SSA; V_t: total pore volume; V_{micro}: micropore volume; C_s: specific capacitance of electrode materials; E: energy density; W: power density; *Cc* carbon cotton; CFs: carbon fibers; CC: carbon cloth; rGO: reduced graphene oxide; EMITFSI: 1-ethyl-3-methylimidazolium bis(trifluoromethylsulfonyl) imide; TEABF4: tetraethylammonium tetrafluoroboratet.

for the chemical properties of the carbon materials [118,184,185]. The active materials are filtered through filter membranes (PTFE, PVDF) [186] to form a hybrid free-standing film. This method resolves the low mass loading and packing density of flexible electrodes for supercapacitors, and simplifies the device fabrication processes [139,187,188]. Furthermore, it allows facile control over the stacked films thickness via simply varying the concentration of dispersion solution or the filtration volume [138]. Compared with vacuum filtration, a dead-end tube membrane (DETM) ultrafiltration is adopted, by which residual solvent can be removed faster with low-cost consumption and environmentally friendly [120,137,189]. This filtration process not only obviously accelerates the filtering time, but produces densely compacted and deposited film under high pressure of 2 MPa [190]. Therefore, the filtration-assisted film displays great potential for self-supported flexible film electrode materials.

3. Biomass derived free-standing electrode materials for high performance supercapacitors

As a result of merits in biocompatibility, abundance and low-cost, biomass is considered as a potential precursor for carbons materials in energy storage devices. Table 1 summarizes strategies of carbonization or pyrolysis to prepare carbon-based electrode materials and information of the heteroatom content, fabricating conditions, and electrochemical performance corresponding with the biomass derived free-standing electrodes.

3.1. Cotton derived free-standing carbon materials

Cotton composed of >90% entangled microscale cellulose fibers is sustainable and abundant in nature, which is a flexible material for preparing carbon-based aerogels by thermally treated [198,231]. Meanwhile, it offers excellent processability that can be spun into extended fibers and easily weaved into fabric with complicated textures and porosities. Carbonized cotton fibers have good conductivity, robust mechanical properties and structural disposability, which makes them as lightweight electrode materials for wearable electronics [130].

Activated carbonized cotton fiber (ACC)-rGO composites suggest great potentials in the commercialization of portable electronic devices [192]. The ACC-rGO were fabricated through vacuum filtration of ACC-graphene oxide (GO) mixed suspension, then immersed in hydroiodic acid followed by calcination at 300 °C under Ar/H_2 mixed atmosphere. Interestingly, embedding ACC into the nanosheets of rGO film successfully regulated the chemical composition and prevents the GN sheets from aggregation (Fig. 5a and b). With the increase mass of ACC, the SSA increased gradually. In comparison with other mass ratios of ACC: GO, ACC-rGO-2 ($m_{(ACC)}$: $m_{(GO)}$ = 1: 1) presented a relatively larger specific surface area of 396.2 $m^2 g^{-1}$ and an average micropore size about 0.5 nm. It showed increased capacitance of 310 $F g^{-1}$ at 0.1 $A g^{-1}$ in 6 M KOH solution, compared to neat rGO film of 100 $F g^{-1}$ at the same conditions. The devices based on ACC-rGO-2 films have different layers fabricated as depicted in Fig. 5c. Cyclic Voltammetry (CV) curves (Fig. 5d) showed superior electrochemical response with increase of film layers, which was consistent with areal capacitance behavior in Fig. 5f. This supercapacitor presented areal capacitance of 1.71 $F cm^{-2}$ at 1.6 $mA cm^{-2}$. However, there were no obvious difference between these three in gravimetric capacitance (Fig. 5e).

In order to address the difficulty of efficient energy storages combined with a minimum carbon footprint, carbonization and CO_2 activation steps were utilized to manufacture an ultra-microporous activated carbon cloth [230]. Kostoglou and his co-workers certified that the full-cell displayed a gravimetric

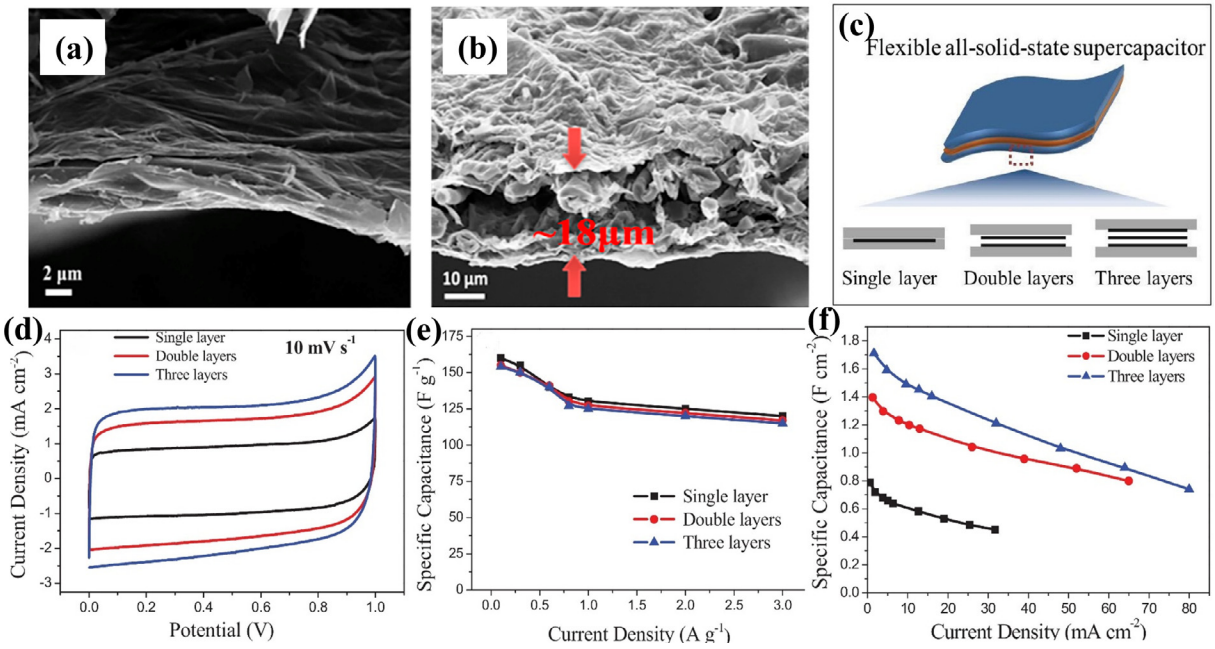

Fig. 5. (a, b) Cross-section field emission scanning electron microscope (FESEM) images of rGO and ACC-rGO composite membranes. (c) Scheme of the procedures for SCs. (d) CV curves of the flexible devices at 10 mV s^{-1}. (e, f) Gravimetric capacitance and areal capacitance for SCs with different layers [192].

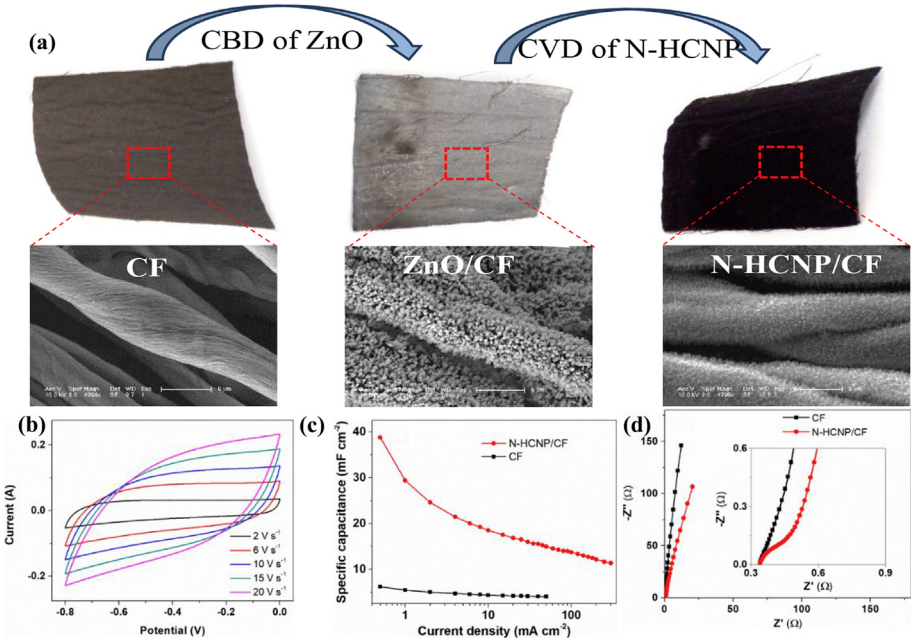

Fig. 6. (a) Illustrations for the preparing procedure of N–HCNP/CF. (b) CV curves of N–HCNP/CF as a function of scan rate. (c) Specific areal capacitances of N–HCNP/CF and CF as a function of current density. (d) Electrochemical impedance spectroscopy (EIS) of N–HCNP/CF and CF electrodes, inset depicts the EIS at high-frequency region [195].

capacitance of 121 F g^{-1} at current density of 0.02 A g^{-1}. The results were closely relative to the material's SSA of 1205 m^2 g^{-1}. This SSA value was superior to that of commercial available AC. Furthermore, the SCs remained over 97% of initial capacitances after 10,000 charge-discharge cycles, contributing to their ultra-micropore size about 0.6 nm of the AC cloth.

An omissible template-removing step synthesis approach has been applied in preparation of a binder-free carbon composite that N-doped hollow hexagonal nanoprism (N–HCNP) is in situ deposition with ZnO template on carbonized fiber cloth substrate (Fig. 6a) [195]. The optimized $KMnO_4$ concentration of 1 mM achieved activated and compacted arrays of carbon cloth to ensure the high areal capacitance of the composite electrode material. Meanwhile, the in situ deposition of N–HCNP on carbon fiber and open channel architecture of arrays led to low interface resistance which remarkably promoted the rapid electron transfer. Owing to these above structural advantages, the resultant N–HCNP/CF displayed high areal capacitance of 38.8 mF cm^{-2} at 0.5 mA cm^{-2} and outstanding rate performance as the CV curve kept quasi-rectangular shape even at a high scan rate of 20 V s^{-1} (Fig. 6b and

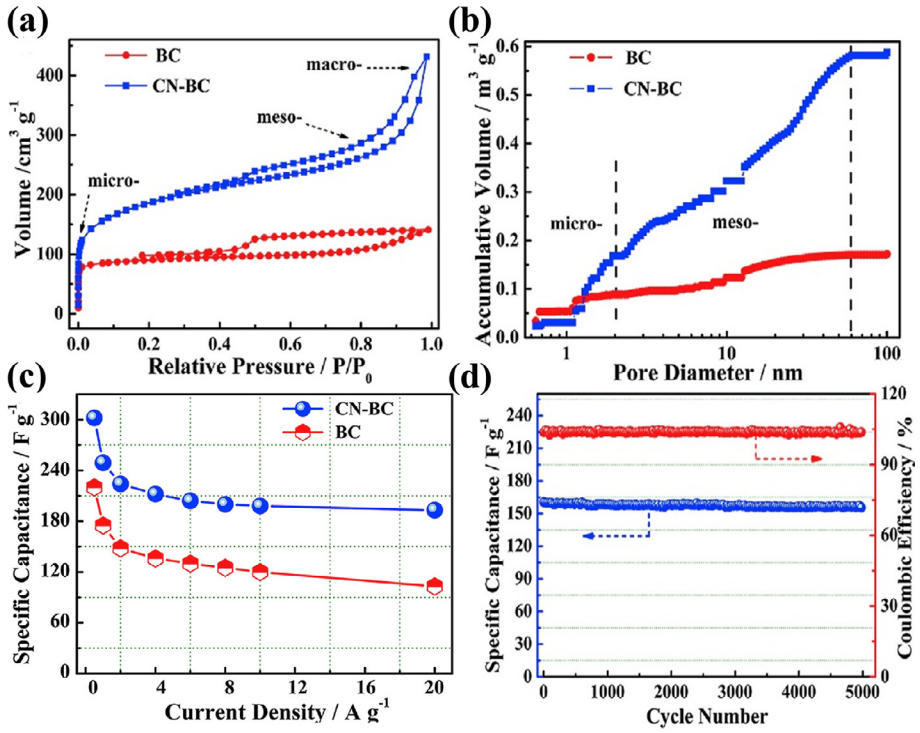

Fig. 7. (a) N_2 adsorption/desorption isotherms and (b) PSD of BC and CN-BC. (c) Specific capacitances at different current densities. (d) Cycling stability for CN-BC at a current density of 2 A g^{-1} [200].

c). As shown in Fig. 6d, the faradaic resistance below 0.6 Ω further certified the low resistance of N–HCNP/CF. As a self-supported and flexible material in EDLCs, the nitrogen-doped carbonized cotton has been reported in CVD system under the flowing mixture of Ar and NH_3 and subsequent carbonization at 800 °C [196]. The carbon product carbonized for 1 h demonstrated the highest capacitance values of 207 F g^{-1} at 1.0 A g^{-1} in contrast with the counterparts of 0.5 h and 2 h. In addition, the energy density and power density of the capacitor were 7.2 Wh kg^{-1} and 3.823 kW kg^{-1} respectively, because of the synergistic effects of the microporous structure and nitrogen-doped. The flexible SCs also showed good stability with capacitance increased by 34% after 10,000 cycles.

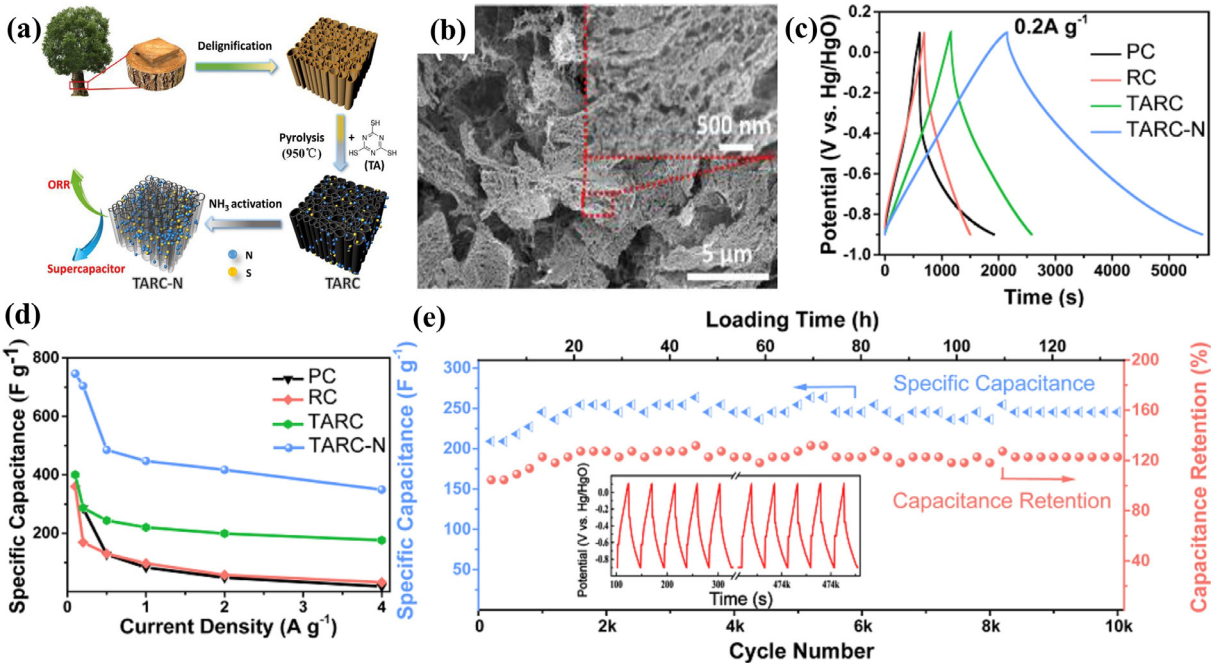

Fig. 8. (a) Illustrations for the fabricating process of TARC-N. (b) SEM image of NH_3 activated carbonized wood carbons. (c) GCD curve at 0.2 A g^{-1}. (d) Specific capacitance of the wood carbon samples at different current densities. (e) Cycling stability for TARC-N at 5 A g^{-1} (inset is first and last 5 cycles) [225].

3.2. Cellulose derived free-standing carbon materials

Hao et al. successfully fabricated interconnected meso-microporous CNFs through heat-treatment of BC [200]. The synthesized CNFs displayed interconnected 3D networks and high degree of graphitization. As shown in Fig. 7a and b, the as-prepared confine nanospace (CN)-BC electrode displayed nitrogen adsorption/desorption isotherm with a steeper increase than pure BC at very low pressure, indicating large numbers of micropores and mesopores. In addition, the obvious increase in N_2 adsorption of CN-BC at $P/P_0 > 0.9$, demonstrating the formation of macroporous carbon. The obtained hierarchical porous structure was facilitated to charge accumulation, fast ion diffusion and reservoirs. Compared to the pure BC electrode material, the BET surface area of CN-BC increased from 302 to 624 $m^2 g^{-1}$ and the pore volume increased from 0.218 to 67 $cm^3 g^{-1}$. Correspondingly, a maximum capacitance of 302 F g^{-1} was measured on the CN-BC at 0.5 A g^{-1} (Fig. 7c), much higher than pure BC of 220 F g^{-1}, benefiting from the effects of porous structure and large ion-accessible surface areas on the electrochemical capacity. The cycling stability of CN-BC device was further evaluated using the galvanostatic charge–discharge (GCD) tests. It was confirmed that the device retained 97% capacitance after 5000 cycles (Fig. 7d). Moreover, a power density of 0.128 kW kg^{-1} could be achieved in aqueous electrolyte solution.

As depicted in Fig. 8a and b, Nitrogen and sulfur doped wood carbons (TARC-N) with low-tortuosity, multichannel and uniformly distributed nanoscale mesopores on carbon wall was prepared from basewood via carbonization and NH_3 activation. [225] The SSA of TARC (without activated) samples was below 200 $m^2 g^{-1}$ and pore volume was less than 0.22 $cm^3 g^{-1}$, demonstrating the macroporous characteristics of wood carbons. In contrast, owing to the anisotropic structure for efficient pathways, the prepared TARC-N brought an optimized BET surface area of 1438 $m^2 g^{-1}$ and pore volume increased to 1.36 $cm^3 g^{-1}$. The capacitance of TARC-N exhibited a high capacitance value of 704 F g^{-1} at 0.2 A g^{-1} in 4 M KOH aqueous solution and kept 122% retention after 10,000 GCD cycles (Fig. 8c–e).

Li and co-workers reported a facile approach to fabricate ultrathin carbon nanofiber aerogels with 3D porously conductive structures [146]. This CNF aerogels produced via a catalytic pyrolysis of nano-cellulose guarantee its inherent nanofibrous morphology. Benefiting from those unique structures, a good electrical conductivity of 710 S m^{-1}, a high capacitance of 90 F g^{-1} and a considerable rate performance of 64% was achieved at very high current density of 100 A g^{-1}. A maximum power density was estimated to be 48.6 kW kg^{-1} that was superior than most reported free-standing carbon-based SCs. The cellulose paper with single-walled carbon nanotubes (SWNTs) for all paper flexible supercapacitor was mediated by coffee green activation and carbonization [86]. Owing to an important role of potassium ions in promoting pyrolytic kinetics and creating well-developed micropores, the device had an improved specific capacitance of 131 F g^{-1} at mass loading of 0.8 mg cm^{-2} over the 64 F g^{-1} originated from the carbonization of a pristine paper towel, and no apparent capacitance loss could be observed (>89%) after 5000 cycles.

3.3. Lignin derived free-standing carbon materials

A sustainable and inexpensive approach had been reported to convert lignin into free-standing and flexible carbon fiber electrodes with ultrafast energy storage [209]. The porous carbon fibers with scale of submicron diameter were fabricated by electrospun and subsequently partial gasification during carbonization. O_2-activation allowed to deliver not only a high BET surface area of 1005 $m^2 g^{-1}$, but an electroactive surface chemistry. Interestingly, although the capacitance of the cell only reached at 45 F g^{-1}, the good electrochemical capacity in power energy of 61 kW kg^{-1} was comparable to the top engineered structures. The cycling lifespan of CFs was excellent on 100,000 cycles and could practically maintain around 90% of initial capacitance. In addition, lignin-derived carbon monolith had been synthesized through a dual template approach [214]. On one hand, this new method provided desirable microstructure, and it was beneficial to efficient ion diffusion and electrical conduction. On the other hand, hierarchically porous structure had high electrical conductivity, which simultaneously realized good areal and volumetric capacitances of 3.0 F cm^{-2} and 97.1 F cm^{-3} at a high mass loading of 14.4 mg cm^{-2}.

Electrospun lignin derived carbon nanofiber mats fabricated through carbonization had features of the small average pore width, large pore volume and high surface area [145]. Increasing the mass ratio of lignin to PVA would lead to an increase of SSA from 14 to 583 $m^2 g^{-1}$ and the average pore size of the carbon mats decreased from 19.4 to 3.5 nm. The as-prepared nanofibers displayed a gravimetric capacitance of 50 F g^{-1} at 2 A g^{-1} and only reduced by 10% after 6000 cycles. Likewise, the nano-structure and morphologies of electrospun fibers were strongly controlled by the carbonization and activation conditions. For instance, electrospun Kraft lignin fibers had relatively uniform diameter of 769 nm with smooth and dense structures (Fig. 9a) [211]. Followed by carbonization and additional activated steps, the morphology of carbon fiber mats did not change. However, those treatments gave average diameter decrease to 567 nm and had cylindrical shape of randomly entangled fibers as depicted in Fig. 9b. It could be observed in Fig. 9c that CV curves showed the rectangular shape of EDLCs at a high scan rate of 1 V s^{-1}. A slight curvature indicated pseudo-capacitive attributed from oxygen and nitrogen functional groups. Compared with CO_2-activated sample, the carbon fibers without activation possessed a distorted rectangular shape due to their excess of ultra-micropores. Hence, the free-standing microporous carbon mats displayed an outstanding rate performance of 113 F g^{-1} at very high current density of 250 A g^{-1} (Fig. 9d).

3.4. Silk derived free-standing carbon materials

The nature silk cocoon with robustly fibrous protein structure has become a significant bio-material. It has great biocompatibility, ease of processing, thermo-electrical and photo-protective properties. In theory, silk fiber has nitrogen content of 18%, and thus its carbonized products are nitrogen doped. In contrast with other natural fibers, this biopolymer with good mechanical properties is commonly applied in high quality textile industries and for flexible devices [232]. 1D hierarchically porous carbon microfibers originating from silk cocoon were fabricated by electrospun and subsequent carbonization [233]. It was believed that this biopolymer as carbon source facilitated to avoid utilizations of abundant hazardous organic solutions in the synthetic processes. The microfibers with 6 μm diameter were consisted of carbon nanoparticles with 10–40 nm diameters. Owing to this specific structure, the sample exhibited a high surface area of 800 $m^2 g^{-1}$ and a capacitance as high as 215 F g^{-1} in 6 M KOH, which proved to be potential for free-standing electrodes.

In order to resolve the inherent restricts of CNTs with their relatively low surface area and low capacity, acid-assisted free-standing carbon composite paper electrodes (FCCPEs) have been prepared through the processes as illustrated in Fig. 10a [234]. FCCPEs combined acid treated CNTs with heteroatom doped carbon nanoplate (H-CMNs) obtained from carbonization of the silk fibroin film. The FE-SEM image depicted that the carbon composites had a rough surface with random orientation of FCCPEs (Fig. 10c). Due to

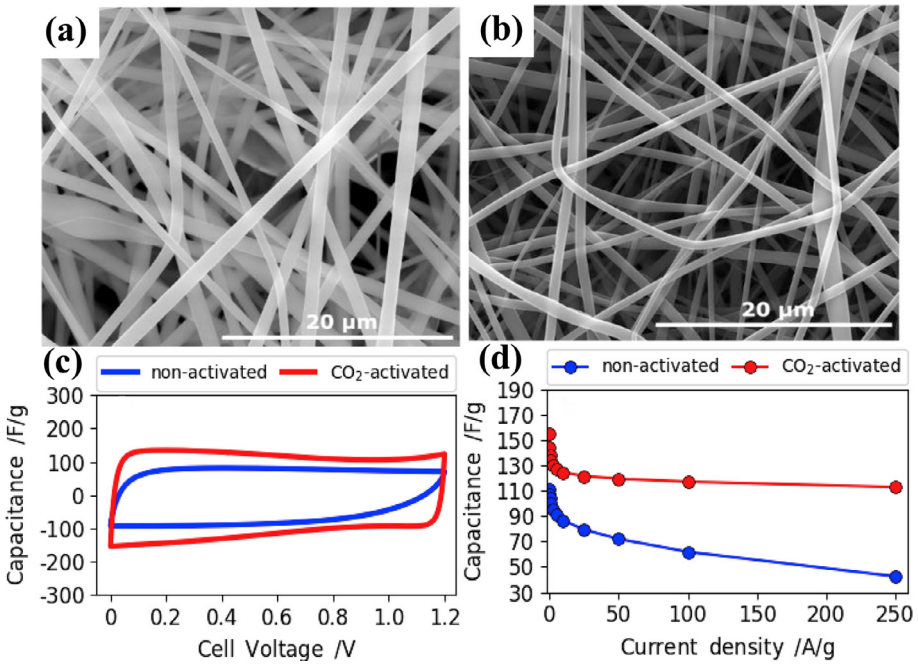

Fig. 9. (a) The electrospun fiber mats prepared from lignin. (b) Carbonized and activated mats. (c) CV curve at scan rates 1 V s^{-1} for non-activated and CO_2-activated carbon fiber electrode materials. (d) Dependence of specific gravimetric capacitance on different current densities [211].

the tight binding provided by CNTs (Fig. 10e), the obtained film was flexible (Fig. 10b). Fig. 10d showed that composites had obviously improved SSA of 1211.7 $m^2 g^{-1}$, which was much higher than the value of 112.2 $m^2 g^{-1}$ for CNTs. The nano-hybrid electrode composites displayed a specific capacitance of 148 F g^{-1} (Fig. 10f and g). Accordingly, a specific energy of 63 Wh kg^{-1} at a power density of

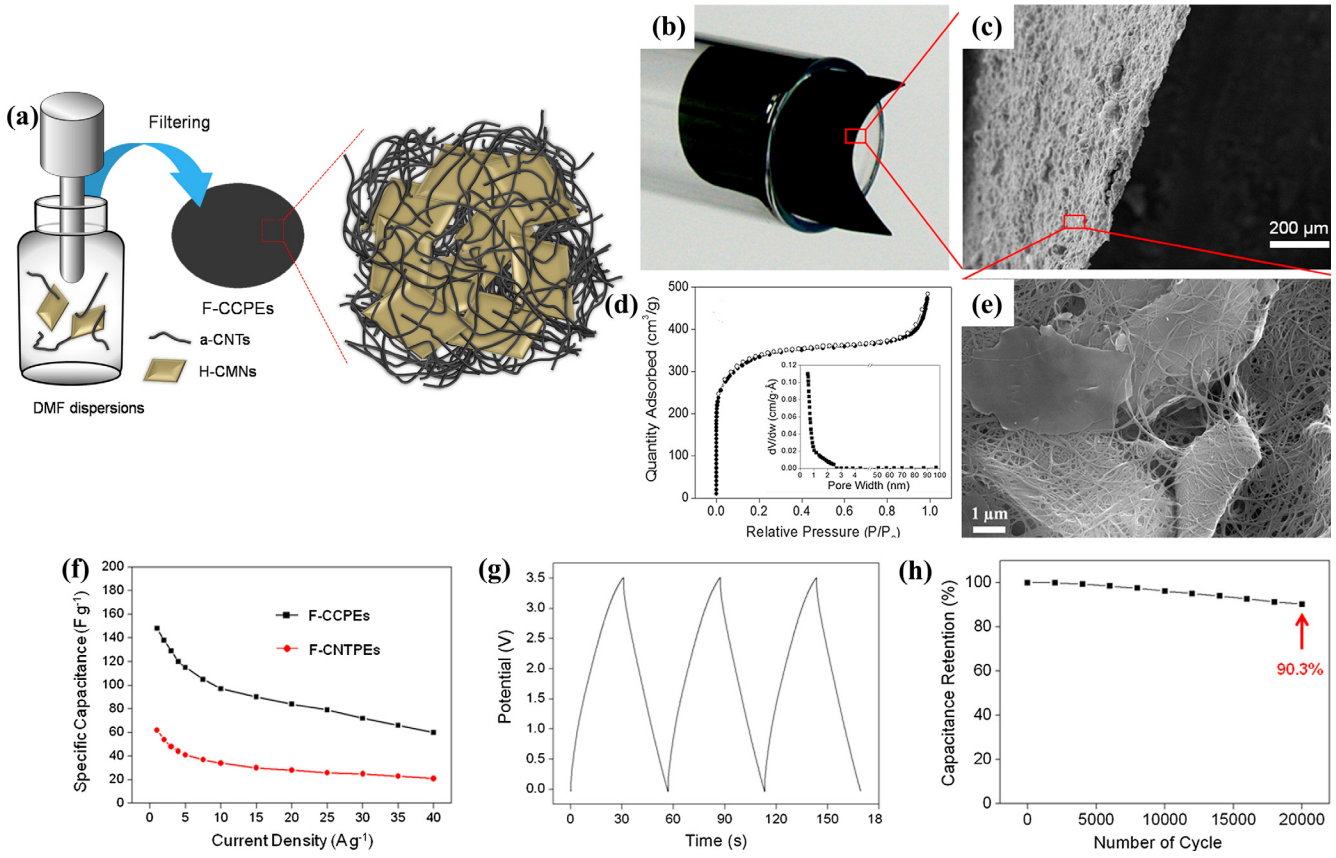

Fig. 10. (a) A scheme of the processes for preparing FCCPEs. (b) Optical image, (c) Fe-SEM, (d) nitrogen adsorption–desorption isotherm and (e) FE-SEM images of F-CCPEs. (f) Specific capacitance of F-CCPEs as a function of current density. (g) GCD curve of the prepared electrode materials. (h) Capacitance retention of F-CCPEs as a function of numbers of cycle in organic electrolyte [234].

140 kW kg^{-1} and outstanding cycling stability of 20,000 cycles were achieved in organic electrolytes (Fig. 10h).

Recently, a free-standing graphene doped with high N content of 15% (NDG) from silk cocoon film was fabricated though pyrolysis of the cocoon at high temperature in argon atmosphere [235]. Inverse proportion between the concentration of nitrogen and processing temperature, led to the higher conductivity and capacitance capacity at relatively low temperature. The NDG pyrolyzed at 400 °C possessed highest capacitance of 220.5 F g^{-1} at 0.8 A g^{-1} and electronic conductivity of 3.8×10^{-2} S m^{-1}, compared with 37.6 and 18.0 F g^{-1}, 9.5×10^{-5} and 1.6×10^{-6} S m^{-1} for the counterparts of 600 and 800 °C, respectively. Furthermore, the SC device achieved high energy density of 9.8 Wh kg^{-1} and a power density of 9.9 kW kg^{-1} in 1 M H_2SO_4 aqueous solution. Those above enhanced performances were mainly because of the high electronegativity of nitrogen which formed dipoles on surface layer of NDG. Therefore, these dipoles improved the capacity of graphene to attract charged species to its surface.

3.5. Carbohydrate derived free-standing carbon materials

Polymer-derived 3D strutted graphenes (SGs) have been developed via a sugar-blowing route in recent years [236]. However, the fabricating process derived from glucose precursor needed to be improved because of the drawbacks in low operation voltage about 1 V. Thereby, sucrose precursor derived GN fabricated through ammonium-assisted chemical blowing and annealing at 1400 °C, were proposed for large-scale production [219]. Owing to the sponge-like solid foams of SG, the stacking density of the SG was about 3–10 mg cm^{-3}. GN films were prevented from agglomeration state via supports of the strutted bubble structures, therefore they achieved the large surface area of 710 m^2 g^{-1}. Depended on the aforementioned interconnected structure, the resultant SCs realized the good rate performance of 58 F g^{-1} at extremely high current density of 100 A g^{-1} and a maximum power density of 340 kW kg^{-1}.

It has been reported that a simple assemble process was applied to prepared starch-based self-supported electrode materials [217]. KOH was used as an activated agent to tune the porosity of electrodes under the heat-treatment. Hence, different ratios of KOH showed an effective influence on samples (marked F-AC-X, in which X represented the mass (g) of potassium hydroxide). Fig. 11a and b isotherms showed SSA and the pore volume of F-AC-X were increased with the increasing of KOH content. BET surface area was 63.66 and **77.**34 m^2 g^{-1} and total volume values of 0.028 and 0.045 cm^3 g^{-1} for as-synthesized F-AC-3 and F-AC-6, respectively. Compared with these counterparts, the F-AC-12 had highest values of 0.058 cm^3 g^{-1} and 1367.87 m^2 g^{-1}. It was believed that the improved SSA of the F-AC-12 was attributed to micropores of the carbon film on the carbon cloth substrate. Furthermore, electrochemical measurements demonstrated that the average specific capacitance of the F-AC-X synchronously elevated with the increase of KOH mass. The resultant F-AC-12 electrode achieved the maximum gravimetric capacitance of 272 F g^{-1} at 1 A g^{-1} in 6 M KOH aqueous solution, and a good rate performance up to 75.9% initial capacitance at 50 A g^{-1} (Fig. 11c and d). Such superior electrochemical performances of F-AC-12 were contributing from abundant opening porous structures, which led to rapid pathways for electron transfer. Similar to as mentioned bio-polymers, chitosan, another renewable biomass, is widely distributed, low-cost and simultaneously with large amounts of element carbon and nitrogen. It has become a promising alternative to fossil resources for manufacturing N-doped carbons applied in energy fields [237]. 3D hierarchical porous N-doped carbons with fiber-wall interconnected architectures, were obtained via dissolving-gelling method and following carbonization [223]. A nanofibrous interconnected network was produced under the aggregation of chitosan chains after gelling treatment, and then the samples were pyrolyzed at 800 °C for 2 h under N_2 atmosphere to obtain carbon aerogels. Nanorod carbons with hierarchical structures gave an excellent specific capacitance of 261 F g^{-1} at 0.5 A g^{-1} and low ESR of 1.24 Ω.

3.6. Other biomass derived free-standing carbon materials

In addition to above mentioned biomass materials, chitin have

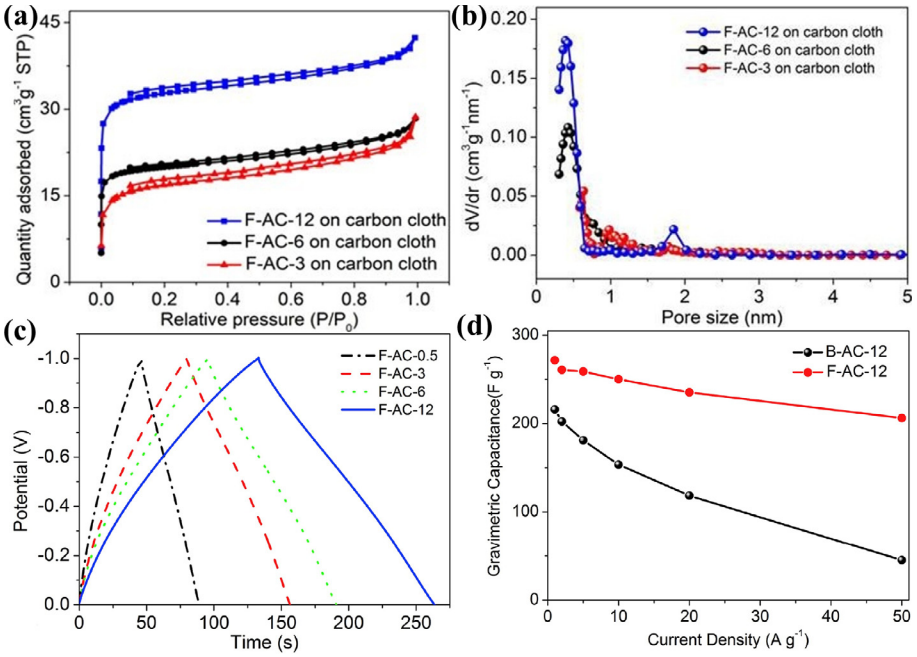

Fig. 11. (a) Nitrogen adsorption-adsorption isotherms (b) PSD of the F-AC-3, 6, 12 samples. (c) GCD curves of as-prepared electrodes at 2 A g^{-1}. (d) Gravimetric capacitances as a function of current density [217].

also been applied as a precursor in porous carbon, while few have been investigated for supercapacitor electrode materials. Chitin is the main structural component in the shells of crabs, shrimps, insects and the cell walls of fungi, which contains 6.9 wt% N from N-acetyl groups. Mesoporous N-doped carbon film with a layered architecture had been fabricated via sol-gel condensation, carbonization and etched silica [228]. Nanocrystalline chitin was used both as a soft template and C, N sources in the fabricating processes. The varied silica concentrations of the composite change its pore size, surface area, structural ordering, etc. However, the pores of carbon could partly damage under high content of silica due to the poor connectivity between carbon regions, while low silica loading did not create developed mesopores. The optimized mesopores were achieved in the silica concentration of 23 wt%, which delivered the largest SSA of 1000 $m^2 g^{-1}$ and pore volume of 0.88 $cm^3 g^{-1}$. The specific capacitance of the optimal sample was 183 F g^{-1} at current densities of 230 mA g^{-1}. Gelatin, a renewable and non-toxic biomass resource with rich $-NH_2$ and $-OH$ groups [238–240], has also been reported as precursor to prepare porous film. As-prepared N-doped thin carbon films (NCF) were successfully fabricated by carbonization of gelatin/HKUST-1 (a metal organic framework made up of copper nodes) composites and subsequent removal of copper compounds [226]. The as-prepared sample heated under 900 °C (NCF-900) delivered the superior electrochemical performance in specific capacitances of 168 F g^{-1} at a current density of 5.0 A g^{-1}, compared with 143.5 and 126.3 F g^{-1} for the counterparts NCF-600 and NCF-800 electrodes at same conditions, respectively. This film electrode achieved an outstanding electrochemical stability, and there was no obvious capacitance degradation after 11,000 cycle tests.

As byproducts of starch processing, zein and hordein are the two widespread nitrogen-rich plant proteins [241–243]. Nanofibers originating from a mixture of these two proteins have been reported using electrospinning technology. The obtained protein fabrics contain about 16% nitrogen and display good tensile strength, controllable diameter, well-defined porous structure, etc. [244–247] Wang and co-workers successfully synthesized nitrogen-doped ultrafine carbon nanofibers by addition of Zn^{2+} and Co^{2+} (hz-ZnX, and hz-CoX where X represented Zn/Co concentrations in suspension of 0.1, 0.2, and 0.3 M) through electrospinning and carbonization [248]. As shown in Fig. 12a, the electrospun protein fibers with Zn^{2+} and Co^{2+} showed light yellow and pink colors, respectively, and formed free-standing carbon films after carbonization. Some nanoparticles could be observed on the surface of hz-Zn-0.3 fibers (Fig. 12b). Those granules disappeared by using hydrochloric acid (hz-Zn-0.3-p), and thus the fiber displayed a smooth surface and a network of graphitic layers in Fig 12c–d. Transition metal ions were introduced into electrospun fibers in order to facilitate stronger interactions among protein molecules and afford solid support to avoid sharp shrinkage of fibers, which induced the formation of graphitic layers during carbonization. Those features enhanced the wettability of electrode/electrolyte and promoted the migration of electrolyte ions, thus rendering better electrochemical capacities to the film. The free-standing carbon film delivered specific capacitance of 393 F g^{-1} at 1 A g^{-1}, and the value was higher than hz-Co-0.2-p of 291 F g^{-1} at the same conditions (Fig. 12e and f). The retention capability of hz-Zn-0.3-p maintained 97.8% after 2000 cycling tests (Fig. 12g).

4. Summary and perspective

This review summarizes the progress in renewable resources derived free-standing electrode materials for high performance SCs. In terms of electrochemical performance, versatile strategies of regulating the porous architecture, chemical/physical activation, and heteroatom doping have been presented. Covering from the methods of fabricating binder-free carbonaceous materials such as gelation, electrospinning, vacuum filtration, etc., to discussions of free-standing carbon electrodes used for supercapacitors. The capability to design the supercapacitor devices on the basis of expected power/energy demand, allows them to become potential alternatives to conventional capacitors and LIB. Although the great achievements have been obtained, many challenges are still remained in preparing biomass-based free-standing electrode

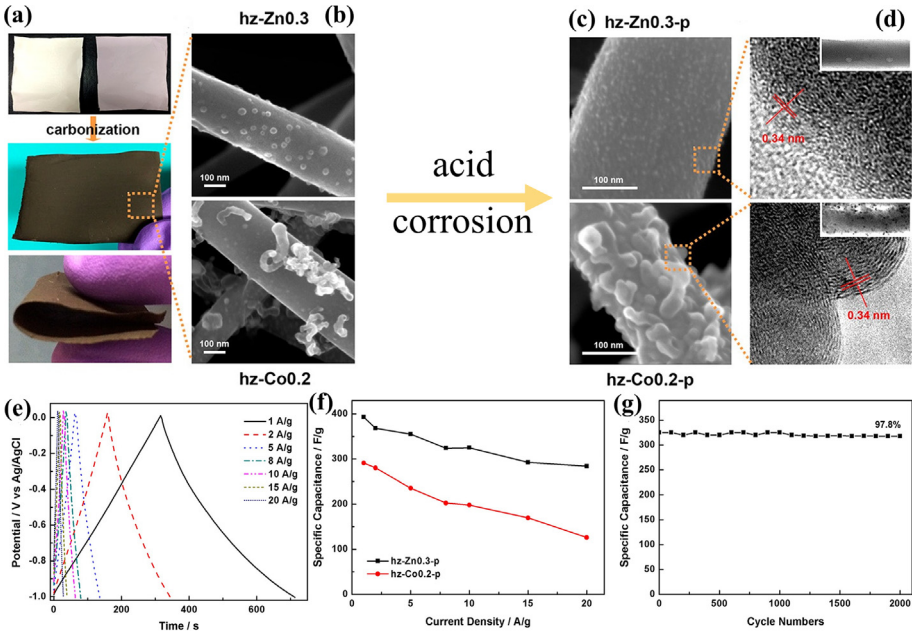

Fig. 12. (a) Digital images of as-spun fibers hz-Zn0.3 and hz-Co0.2 before and after carbonization. (b) SEM images of hz-Zn0.3 and hz-Co0.2 and (c) corresponding samples after hydrochloric acid treatment. (d) Transmission electron microscope (TEM) images of hz-Zn0.3-p and hz-Co0.2-p. (e) GCD curves of hz-Zn0.3-p at different current densities. (f) Specific capacitances of hz-Zn0.3-p and hz-Co0.2-p at various current densities. (g) Specific capacitances of hz-Zn0.3-p as a function of current density [248].

materials within the current technologies:

Biomass-based Materials: More and more natural originated resources have played a key role in optimizing already existing structures and used for novel energy sources. As sustainable alternatives of common synthetic organics, biomass derived materials and biopolymers have shown a great promise to prepare commercial products for their wide distribution, inexpensive and capacity of biodegradability. Nowadays, many researches have been performed on aspects of carbon precursors, however, only little carbon precursors could be regarded in free-standing carbon materials among many natural organic materials. For the purpose of manufacturing binder-free electrode materials, not only its texture and rheological parameters, but the chemical/physical properties should also be considered. It is inevitable to face the difficulty that how to deal with the inherent limitations of raw materials. Hence, choosing suitable design strategies and uncomplicated processing methods seems to be essential.

Surface characteristics: The size, porous structure, and uniform morphologies of nano-materials are significant parameters in elevating the capacitance performance. In order to guarantee sufficient active loading, the PSD should fulfill the requirements of suitable size of electrolyte ions. While, chemical and physical activation are taken to optimize the porosity. For hierarchical porous structure combining with different size pores, it has been demonstrated the superiority in aspects of shortening ions diffusion and migration pathways. In addition, heteroatom doping or introducing functional groups have been employed to strengthen electrochemical performance of electrodes. It is anticipated that heteroatom doping of carbon materials promotes pseudocapacitance of electrode via an efficient and fast charge transfer between electrodes and electrolytes.

Challenges: Numerous efforts have been devoted to fabricating flexible energy storage devices with idealized performance. However, plenty of current challenges still hamper their fundamental researches and large-scale commercial applications. To fabricate flexible electronics with good mechanical properties and outstanding electrochemical capacities, metal foil and stainless steel grids are commonly used for loading of active materials. But, these electrode materials are usually corroded in acid/alkaline electrolytes, which limits the service life of devices. And it is also difficult to fabricate flexible carbon electrode materials with tailored architectures on a large scale and in a cost-efficient approach. Additionally, majorities of the flexible and free-standing carbon electrodes suffer from their low capacitance and low energy density: EDLCs are limited by energy density about 5–20 Wh kg^{-1} by contrast with PCs about 40–100 Wh kg^{-1} and LIB around 120–170 Wh kg^{-1}. It means the difficulties in meeting the needs of practical production applications.

In summary, it is a promising developing direction of sustainable and biomass derived materials, and thus the research target should be oriented toward high electrochemical performance, good mechanical properties and free-standing supercapacitors. The deposition or embedding CNTs (GN) onto flexible or stretchable substrates and the construction of free-standing carbon materials through simple one-step carbonization and activation preparation processes, are the two main strategies to fabricate highly conductive and flexible carbon electrode materials. These prepared SCs show markedly optimized energy density without compromising their power capacity. Furthermore, biomass-based binder-free SCs will promote the progress of this good prospect field of electrical energy storage, and find ways of realizing its practical application in the near future.

Acknowledgements

National Natural Science Foundation of China (No. 21774060), National Key R&D Program of China (2017YFF0207804), Jiangsu key lab of biomass-based energy and Materials (JSBEM2016011), State Key Laboratory for Mechanical Behavior of Materials (20171914), Priority Academic Program Development of Jiangsu Higher Education Institutions (PAPD), Top-notch Academic Programs Project of Jiangsu Higher Education Institutions (TAPP) and Natural Science Key Project of the Jiangsu Higher Education Institutions (16KJA220006) are acknowledged with gratitude. We also thank Advanced Analysis & Testing Center, Nanjing Forestry University for SEM characterization.

References

[1] A. Burke, Ultracapacitors: why, how, and where is the technology, J. Power Sources 91 (1) (2000) 37–50.
[2] J. Xue, T. Wu, Y. Dai, Y. Xia, Electrospinning and electrospun nanofibers: methods, materials, and applications, Chem. Rev. 119 (8) (2019) 5298–5415.
[3] C. Liu, F. Li, L.P. Ma, H.M. Cheng, Advanced materials for energy storage, Adv. Mater. 22 (8) (2010) E28–E62.
[4] H. Yang, S. Liu, L. Cao, S. Jiang, H. Hou, Superlithiation of non-conductive polyimide toward high-performance lithium-ion batteries, J. Mater. Chem. 6 (42) (2018) 21216–21224.
[5] X. Zhao, B.M. Sanchez, P.J. Dobson, P.S. Grant, The role of nanomaterials in redox-based supercapacitors for next generation energy storage devices, Nanoscale 3 (3) (2011) 839–855.
[6] L. Dai, D.W. Chang, J.B. Baek, W. Lu, Carbon nanomaterials for advanced energy conversion and storage, Small 8 (8) (2012) 1130–1166.
[7] M.R. Gao, Y.F. Xu, J. Jiang, S.H. Yu, Nanostructured metal chalcogenides: synthesis, modification, and applications in energy conversion and storage devices, Chem. Soc. Rev. 42 (7) (2013) 2986–3017.
[8] X. Mao, T. Hatton, G. Rutledge, A review of electrospun carbon fibers as electrode materials for energy storage, Curr. Org. Chem. 17 (13) (2013) 1390–1401.
[9] Q. Zhang, E. Uchaker, S.L. Candelaria, G. Cao, Nanomaterials for energy conversion and storage, Chem. Soc. Rev. 42 (7) (2013) 3127–3171.
[10] X. Wang, X. Lu, B. Liu, D. Chen, Y. Tong, G. Shen, Flexible energy-storage devices: design consideration and recent progress, Adv. Mater. 26 (28) (2014) 4763–4782.
[11] J. Yan, Q. Wang, T. Wei, Z. Fan, Recent advances in design and fabrication of electrochemical supercapacitors with high energy densities, Advanced Energy Materials 4 (4) (2014) 1300816.
[12] W. Xu, Y. Ding, Y. Yu, S. Jiang, L. Chen, H. Hou, Highly foldable PANi@ CNTs/PU dielectric composites toward thin-film capacitor application, Mater. Lett. 192 (2017) 25–28.
[13] P. Simon, Y. Gogotsi, Materials for electrochemical capacitors, Nat. Mater. 7 (2008) 845–854.
[14] M. Winter, R.J. Brodd, What are batteries, fuel cells, and supercapacitors? Chem. Rev. 104 (10) (2004) 4245–4270.
[15] Y. Wang, Y. Xia, Recent progress in supercapacitors: from materials design to system construction, Adv. Mater. 4 (37) (2013) 5336–5342, 25.
[16] V. Augustyn, P. Simon, B. Dunn, Pseudocapacitive oxide materials for high-rate electrochemical energy storage, Energy Environ. Sci. 7 (5) (2014) 1597.
[17] P. Simon, Y. Gogotsi, B. Dunn, Materials science. Where do batteries end and supercapacitors begin? Science 343 (6176) (2014) 1210–1211.
[18] S. Zhang, N. Pan, Supercapacitors performance evaluation, Advanced Energy Materials 5 (6) (2015) 1401401.
[19] V. Aravindan, M. Ulaganathan, S. Madhavi, Research progress in Na-ion capacitors, J. Mater. Chem. 4 (20) (2016) 7538–7548.
[20] Y. Wang, Y. Song, Y. Xia, Electrochemical capacitors: mechanism, materials, systems, characterization and applications, Chem. Soc. Rev. 45 (21) (2016) 5925–5950.
[21] G. Wang, L. Zhang, J. Zhang, A review of electrode materials for electrochemical supercapacitors, Chem. Soc. Rev. 41 (2) (2012) 797–828.
[22] Elzbieta Frackowiaka, François Béguinb, Carbon materials for the electrochemical storage of energy in capacitors, Carbon 39 (2001) 937–950.
[23] L.L. Zhang, X.S. Zhao, Carbon-based materials as supercapacitor electrodes, Chem. Soc. Rev. 38 (9) (2009) 2520–2531.
[24] M.D. Stoller, R.S. Ruoff, Best practice methods for determining an electrode material's performance for ultracapacitors, Energy Environ. Sci. 3 (9) (2010) 1294, 5.
[25] Y. Zhang, H. Feng, X. Wu, L. Wang, A. Zhang, T. Xia, et al., Progress of electrochemical capacitor electrode materials: a review, Int. J. Hydrogen Energy 34 (11) (2009) 4889–4899.
[26] B.K. Deka, A. Hazarika, J. Kim, Y.-B. Park, H.W. Park, Recent development and

challenges of multifunctional structural supercapacitors for automotive industries, Int. J. Energy Res. 41 (10) (2017) 1397–1411.
[27] D.A.C. Brownson, D.K. Kampouris, C.E. Banks, An overview of graphene in energy production and storage applications, J. Power Sources 196 (11) (2011) 4873–4885.
[28] X. Huang, Z. Zeng, Z. Fan, J. Liu, H. Zhang, Graphene-based electrodes, Adv. Mater. 24 (45) (2012) 5979–6004.
[29] M. Inagaki, H. Konno, O. Tanaike, Carbon materials for electrochemical capacitors, J. Power Sources 195 (24) (2010) 7880–7903.
[30] L.Y. Zhang, S.J. He, S.L. Chen, Q.H. Guo, H.Q. Hou, Preparation and electrochemical properties of polyaniline/carbon nanofiber composite materials, Acta Phys. - Chim. Sin. 26 (12) (2010) 3181–3186.
[31] Y. Zhai, Y. Dou, D. Zhao, P.F. Fulvio, R.T. Mayes, S. Dai, Carbon materials for chemical capacitive energy storage, Adv. Mater. 23 (42) (2011) 4828–4850.
[32] M. Zhi, C. Xiang, J. Li, M. Li, N. Wu, Nanostructured carbon-metal oxide composite electrodes for supercapacitors: a review, Nanoscale 5 (1) (2013) 72–88.
[33] S. He, X. Hu, S. Chen, H. Hu, M. Hanif, H. Hou, Needle-like polyaniline nanowires on graphite nanofibers: hierarchical micro/nano-architecture for high performance supercapacitors, J. Mater. Chem. 22 (11) (2012) 5114.
[34] S. He, L. Chen, C. Xie, H. Hu, S. Chen, M. Hanif, et al., Supercapacitors based on 3D network of activated carbon nanowhiskers wrapped-on graphitized electrospun nanofibers, J. Power Sources 243 (2013) 880–886.
[35] S. He, W. Chen, 3D graphene nanomaterials for binder-free supercapacitors: scientific design for enhanced performance, Nanoscale 7 (16) (2015) 6957–6990.
[36] Y. Huang, J. Liang, Y. Chen, An overview of the applications of graphene-based materials in supercapacitors, Small 8 (12) (2012) 1805–1834.
[37] H. Ma, Q. Zhou, M. Wu, M. Zhang, B. Yao, T. Gao, et al., Tailoring the oxygenated groups of graphene hydrogels for high-performance supercapacitors with large areal mass loadings, J. Mater. Chem. 6 (15) (2018) 6587–6594.
[38] K. Fic, A. Platek, J. Piwek, E. Frackowiak, Sustainable materials for electrochemical capacitors, Mater. Today 21 (4) (2018) 437–454.
[39] D.R. Rolison, J.W. Long, J.C. Lytle, A.E. Fischer, C.P. Rhodes, T.M. McEvoy, et al., Multifunctional 3D nanoarchitectures for energy storage and conversion, Chem. Soc. Rev. 38 (1) (2009) 226–252.
[40] Z. Yu, L. Tetard, L. Zhai, J. Thomas, Supercapacitor electrode materials: nanostructures from 0 to 3 dimensions, Energy Environ. Sci. 8 (3) (2015) 702–730.
[41] S.T. Gao, G.S. Tang, D.W. Hua, R.H. Xiong, J.Q. Han, S.H. Jiang, et al., Stimuli-responsive bio-based polymeric systems and their applications, J. Mater. Chem. B 7 (5) (2019) 709–729.
[42] D. Lv, M.M. Zhu, Z.C. Jiang, S.H. Jiang, Q.L. Zhang, R.H. Xiong, et al., Green electrospun nanofibers and their application in air filtration, Macromol. Mater. Eng. 303 (12) (2018) 18.
[43] D. Lv, R.X. Wang, G.S. Tang, Z.P. Mou, J.D. Lei, J.Q. Han, et al., Ecofriendly electrospun membranes loaded with visible-light responding nanoparticles for multifunctional usages: highly efficient air filtration, dye scavenging, and bactericidal activity, ACS Appl. Mater. Interfaces 11 (13) (2019) 12880–12889.
[44] G.S. Tang, R.H. Xiong, D. Lv, R.X. Xu, K. Braeckmans, C.B. Huang, et al., Gas-shearing fabrication of multicompartmental microspheres: a one-step and oil-free approach, Adv. Sci. 6 (9) (2019) 9.
[45] Z.F. Guo, G.S. Tang, Y.H. Zhou, S.W. Liu, H.Q. Hou, Z.Y. Chen, et al., Fabrication of sustained-release CA-PU coaxial electrospun fiber membranes for plant grafting application, Carbohydr. Polym. 169 (2017) 198–205.
[46] M.M. Zhu, R.H. Xiong, C.B. Huang, Bio-based and photocrosslinked electrospun antibacterial nanofibrous membranes for air filtration, Carbohydr. Polym. 205 (2019) 55–62.
[47] M.M. Pérez-Madrigal, M.G. Edo, C. Alemán, Powering the future: application of cellulose-based materials for supercapacitors, Green Chem. 18 (22) (2016) 5930–5956.
[48] S. He, C. Hu, H. Hou, W. Chen, Ultrathin MnO2 nanosheets supported on cellulose based carbon papers for high-power supercapacitors, J. Power Sources 246 (2014) 754–761.
[49] C. Zheng, Y. Yue, L. Gan, X. Xu, C. Mei, J. Han, Highly stretchable and self-healing strain sensors based on nanocellulose-supported graphene dispersed in electro-conductive hydrogels, Nanomaterials 9 (7) (2019) 937.
[50] Y.Y. Yue, X.H. Wang, J.Q. Han, L. Yu, J.Q. Chen, Q.L. Wu, et al., Effects of nanocellulose on sodium alginate/polyacrylamide hydrogel: mechanical properties and adsorption-desorption capacities, Carbohydr. Polym. 206 (2019) 289–301.
[51] H. Jing-quan, L. Kai-yue, Y. Yi-ying, M. Chang-tong, W. Hui-xiang, Y. Peng-bin, et al., Synthesis and electrochemical performance of flexible cellulose nanofiber-carbon nanotube/natural rubber composite elastomers as supercapacitor electrodes, N. Carbon Mater. 33 (4) (2018) 341–350.
[52] L. Zuo, W. Fan, Y. Zhang, Y. Huang, W. Gao, T. Liu, Bacterial cellulose-based sheet-like carbon aerogels for the in situ growth of nickel sulfide as high performance electrode materials for asymmetric supercapacitors, Nanoscale 9 (13) (2017) 4445–4455.
[53] J.H. Park, H.H. Rana, J.Y. Lee, H.S. Park, Renewable flexible supercapacitors based on all-lignin-based hydrogel electrolytes and nanofiber electrodes, J. Mater. Chem. 7 (28) (2019) 16962–16968.
[54] S. Herou, M.C. Ribadeneyra, R. Madhu, V. Araullo-Peters, A. Jensen, P. Schlee, et al., Ordered mesoporous carbons from lignin: a new class of biobased electrodes for supercapacitors, Green Chem. 21 (3) (2019) 550–559.
[55] S. Leguizamon, K.P. Díaz-Orellana, J. Velez, M.C. Thies, M.E. Roberts, High charge-capacity polymer electrodes comprising alkali lignin from the Kraft process, J. Mater. Chem. 3 (21) (2015) 11330–11339.
[56] J.W. Jeon, L. Zhang, J.L. Lutkenhaus, D.D. Laskar, J.P. Lemmon, D. Choi, et al., Controlling porosity in lignin-derived nanoporous carbon for supercapacitor applications, ChemSusChem 8 (3) (2015) 428–432.
[57] A.G. Pandolfo, A.F. Hollenkamp, Carbon properties and their role in supercapacitors, J. Power Sources 157 (1) (2006) 11–27.
[58] K.S. Sing, Reporting physisorption data for gas/solid systems with special reference to the determination of surface area and porosity (Recommendations 1984), Pure Appl. Chem. 57 (4) (1985) 603–619.
[59] L. Zhang, X. Yang, F. Zhang, G. Long, T. Zhang, K. Leng, et al., Controlling the effective surface area and pore size distribution of sp2 carbon materials and their impact on the capacitance performance of these materials, J. Am. Chem. Soc. 135 (15) (2013) 5921–5929.
[60] Y. Lu, G. Long, L. Zhang, T. Zhang, M. Zhang, F. Zhang, et al., What are the practical limits for the specific surface area and capacitance of bulk sp2 carbon materials? Sci. China Chem. 59 (2) (2015) 225–230.
[61] Y. Lu, S. Zhang, J. Yin, C. Bai, J. Zhang, Y. Li, et al., Mesoporous activated carbon materials with ultrahigh mesopore volume and effective specific surface area for high performance supercapacitors, Carbon 124 (2017) 64–71.
[62] A. Stein, Z. Wang, M.A. Fierke, Functionalization of porous carbon materials with designed pore architecture, Adv. Mater. 21 (3) (2009) 265–293.
[63] T. Liu, Z. Zhou, Y. Guo, D. Guo, G. Liu, Block copolymer derived uniform mesopores enable ultrafast electron and ion transport at high mass loadings, Nat. Commun. 10 (1) (2019) 675.
[64] J. Liu, M. Zhou, L.-Z. Fan, P. Li, X. Qu, Porous polyaniline exhibits highly enhanced electrochemical capacitance performance, Electrochim. Acta 55 (20) (2010) 5819–5822.
[65] H.-F. Ju, W.-L. Song, L.-Z. Fan, Rational design of graphene/porous carbon aerogels for high-performance flexible all-solid-state supercapacitors, J. Mater. Chem. 2 (28) (2014) 10895–10903.
[66] Y. Wang, S. Su, L. Cai, B. Qiu, C. Yang, X. Tao, et al., Hierarchical supercapacitor electrodes based on metallized glass fiber for ultrahigh areal capacitance, Energy Storage Materials 20 (2019) 315–323.
[67] Y. Chen, Z. Xiao, Y. Liu, L.-Z. Fan, A simple strategy toward hierarchically porous graphene/nitrogen-rich carbon foams for high-performance supercapacitors, J. Mater. Chem. 5 (46) (2017) 24178–24184.
[68] S. He, R. Zhang, C. Zhang, M. Liu, X. Gao, J. Ju, et al., Al/C/MnO2 sandwich nanowalls with highly porous surface for electrochemical energy storage, J. Power Sources 299 (2015) 408–416.
[69] C. Merlet, C. Pean, B. Rotenberg, P.A. Madden, B. Daffos, P.L. Taberna, et al., Highly confined ions store charge more efficiently in supercapacitors, Nat. Commun. 4 (2013) 2701.
[70] D. Hulicova-Jurcakova, M. Seredych, G.Q. Lu, T.J. Bandosz, Combined effect of nitrogen- and oxygen-containing functional groups of microporous activated carbon on its electrochemical performance in supercapacitors, Adv. Funct. Mater. 19 (3) (2009) 438–447.
[71] Y. Zeng, X. Li, S. Jiang, S. He, H. Fang, H. Hou, Free-standing mesoporous electrospun carbon nanofiber webs without activation and their electrochemical performance, Mater. Lett. 161 (2015) 587–590.
[72] X. Lu, C. Wang, F. Favier, N. Pinna, Electrospun nanomaterials for supercapacitor electrodes: designed architectures and electrochemical performance, Advanced Energy Materials 7 (2) (2017) 1601301.
[73] F. Rodrıguez-Reinoso, A.C. Pastor, H. Marsh, M.A. Martınez, Preparation of activated carbon cloths from viscous rayon. Part II: physical activation processes, Carbon 38 (3) (2000) 379–395.
[74] Y.-M. Fan, Y. Liu, X. Liu, Y. Liu, L.-Z. Fan, Hierarchical porous NiCo 2 S 4 -rGO composites for high-performance supercapacitors, Electrochim. Acta 249 (2017) 1–8.
[75] T.-T. Chen, W.-L. Song, L.-Z. Fan, Engineering graphene aerogels with porous carbon of large surface area for flexible all-solid-state supercapacitors, Electrochim. Acta 165 (2015) 92–97.
[76] Q. Xie, X. Huang, Y. Zhang, S. Wu, P. Zhao, High performance aqueous symmetric supercapacitors based on advanced carbon electrodes and hydrophilic poly(vinylidene fluoride) porous separator, Appl. Surf. Sci. 443 (2018) 412–420.
[77] D. Liu, K. Ni, J. Ye, J. Xie, Y. Zhu, L. Song, Tailoring the structure of carbon nanomaterials toward high-end energy applications, Adv. Mater. 30 (48) (2018) 1802104.
[78] C. Wang, Y.V. Kaneti, Y. Bando, J. Lin, C. Liu, J. Li, et al., Metal–organic framework-derived one-dimensional porous or hollow carbon-based nanofibers for energy storage and conversion, Materials Horizons 5 (3) (2018) 394–407.
[79] Y.-W. Ju, S.-H. Park, H.-R. Jung, W.-J. Lee, Electrospun activated carbon nanofibers electrodes based on polymer blends, J. Electrochem. Soc. 156 (6) (2009) A489–A494.
[80] X. Qiu, X. Zhang, L.-Z. Fan, In situ synthesis of a highly active Na2Ti3O7 nanosheet on an activated carbon fiber as an anode for high-energy density supercapacitors, J. Mater. Chem. 6 (33) (2018) 16186–16195.
[81] Y. Guo, K. Yu, Z. Wang, H. Xu, Effects of activation conditions on preparation of porous carbon from rice husk, Carbon 41 (8) (2003) 1645–1648.
[82] Y. Guo, S. Yang, K. Yu, J. Zhao, Z. Wang, H. Xu, The preparation and

mechanism studies of rice husk based porous carbon, Mater. Chem. Phys. 74 (3) (2002) 320–323.
[83] Jun'ichi Hayashia, Atsuo Kazehayaa, Katsuhiko Muroyamaa, A. Paul Watkinsonb, Preparation of activated carbon from lignin by chemical activation, Carbon 38 (13) (2000) 1873–1878.
[84] P. Cheng, T. Li, H. Yu, L. Zhi, Z. Liu, Z. Lei, Biomass-derived carbon fiber aerogel as a binder-free electrode for high-rate supercapacitors, J. Phys. Chem. C 120 (4) (2016) 2079–2086.
[85] G.Q. Si Chongdian, Progress research on activation mechanism and regeneration of activated carbon, China Powder Sci. Technol. 14 (5) (2008) 48–52.
[86] D. Lee, Y.G. Cho, H.K. Song, S.J. Chun, S.B. Park, D.H. Choi, et al., Coffee-Driven green activation of cellulose and its use for all-paper flexible supercapacitors, ACS Appl. Mater. Interfaces 9 (27) (2017) 22568–22577.
[87] C. Kim, B.T.N. Ngoc, K.S. Yang, M. Kojima, Y.A. Kim, Y.J. Kim, et al., Self-sustained thin webs consisting of porous carbon nanofibers for supercapacitors via the electrospinning of polyacrylonitrile solutions containing zinc chloride, Adv. Mater. 19 (17) (2007) 2341–2346.
[88] N.D. Kim, S.J. Kim, G.-P. Kim, I. Nam, H.J. Yun, P. Kim, et al., NH3-activated polyaniline for use as a high performance electrode material in supercapacitors, Electrochim. Acta 78 (2012) 340–346.
[89] J. Li, N. Wang, J. Tian, W. Qian, W. Chu, Cross-coupled macro-mesoporous carbon network toward record high energy-power density supercapacitor at 4 V, Adv. Funct. Mater. 28 (51) (2018) 1806153.
[90] H. Jiang, P.S. Lee, C. Li, 3D carbon based nanostructures for advanced supercapacitors, Energy Environ. Sci. 6 (1) (2013) 41–53.
[91] G.Y. Zhou, T.R. Xiong, S.J. He, Y.H. Li, Y.M. Zhu, H.Q. Hou, Asymmetric supercapacitor based on flexible TiC/CNF felt supported interwoven nickel-cobalt binary hydroxide nanosheets, J. Power Sources 317 (2016) 57–64.
[92] M. Pumera, Graphene-based nanomaterials for energy storage, Energy Environ. Sci. 4 (3) (2011) 668–674.
[93] P. Simon, Y. Gogotsi, Capacitive energy storage in nanostructured carbon-electrolyte systems, Acc. Chem. Res. 46 (5) (2013) 1094–1103.
[94] L.-Z. Fan, S. Qiao, W. Song, M. Wu, X. He, X. Qu, Effects of the functional groups on the electrochemical properties of ordered porous carbon for supercapacitors, Electrochim. Acta 105 (2013) 299–304.
[95] S.R. Kelemen MLG, P.J. Kwiatek, Quantification of nitrogen forms in argonne premium coals, Energy Fuel. 8 (1994) 896–906.
[96] Y. Fang, B. Luo, Y. Jia, X. Li, B. Wang, Q. Song, et al., Renewing functionalized graphene as electrodes for high-performance supercapacitors, Adv. Mater. 24 (47) (2012) 6348–6355.
[97] J.P. Paraknowitsch, A. Thomas, Doping carbons beyond nitrogen: an overview of advanced heteroatom doped carbons with boron, sulphur and phosphorus for energy applications, Energy Environ. Sci. 6 (10) (2013) 2839.
[98] R. Liu, L. Ma, G. Niu, X. Li, E. Li, Y. Bai, et al., Flexible Ti-doped FeOOH quantum dots/graphene/bacterial cellulose anode for high-energy asymmetric supercapacitors, Part. Part. Syst. Charact. 34 (10) (2017) 1700213.
[99] Y.X. Liu, X.M. Qiu, X.B. Liu, Y.C. Liu, L.Z. Fan, 3D porous binary-heteroatom doped carbon nanosheet/electrochemically exfoliated graphene hybrids for high performance flexible solid-state supercapacitors, J. Mater. Chem. 6 (18) (2018) 8750–8756.
[100] Y.X. Liu, Z.C. Xiao, Y.C. Liu, L.Z. Fan, Biowaste-derived 3D honeycomb-like porous carbon with binary-heteroatom doping for high-performance flexible solid-state supercapacitors, J. Mater. Chem. 6 (1) (2018) 160–166.
[101] R. Liu, L.N. Ma, J. Mei, S. Huang, S.Q. Yang, E.Y. Li, et al., Large areal mass, mechanically tough and freestanding electrode based on heteroatom-doped carbon nanofibers for flexible supercapacitors, Chem. Eur J. 23 (11) (2017) 2610–2618.
[102] S. He, H. Hou, W. Chen, 3D porous and ultralight carbon hybrid nanostructure fabricated from carbon foam covered by monolayer of nitrogen-doped carbon nanotubes for high performance supercapacitors, J. Power Sources 280 (2015) 678–686.
[103] V. Kuzmenko, O. Naboka, H. Staaf, M. Haque, G. Göransson, P. Lundgren, et al., Capacitive effects of nitrogen doping on cellulose-derived carbon nanofibers, Mater. Chem. Phys. 160 (2015) 59–65.
[104] T. Qin, Z. Wan, Z. Wang, Y. Wen, M. Liu, S. Peng, et al., 3D flexible O/N Co-doped graphene foams for supercapacitor electrodes with high volumetric and areal capacitances, J. Power Sources 336 (2016) 455–464.
[105] F. Su, C.K. Poh, J.S. Chen, G. Xu, D. Wang, Q. Li, et al., Nitrogen-containing microporous carbon nanospheres with improved capacitive properties, Energy Environ. Sci. 4 (3) (2011) 717–724.
[106] B. Xu, S. Hou, G. Cao, F. Wu, Y. Yang, Sustainable nitrogen-doped porous carbon with high surface areas prepared from gelatin for supercapacitors, J. Mater. Chem. 22 (36) (2012) 19088.
[107] a Laboratoire d'Etude et de Caractdrisation des Amorphes et des Polymdres FdS, 76821, Mont-Saint-Aionan Cedex, France b Laboratoire d'Analyses Thermiques, Institut Francais du Pdtrole, BP311, 92506, Rueil-Malmaison Cedex, France. Thermogravimetry/Fourier transform infrared coupling investigations to study the thermal stability of melamine formaldehyde resin, Thermochim. Acta 259 (1995) 143–151.
[108] S. Sepehri, B.B. García, Q. Zhang, G. Cao, Enhanced electrochemical and structural properties of carbon cryogels by surface chemistry alteration with boron and nitrogen, Carbon 47 (6) (2009) 1436–1443.
[109] Z. Peng, R. Ye, J.A. Mann, D. Zakhidov, Y. Li, P.R. Smalley, et al., Flexible boron-doped laser-induced graphene microsupercapacitors, ACS Nano 9 (6) (2015) 5868–5875.
[110] Z.-H. Sheng, H.-L. Gao, W.-J. Bao, F.-B. Wang, X.-H. Xia, Synthesis of boron doped graphene for oxygen reduction reaction in fuel cells, J. Mater. Chem. 22 (2) (2012) 390–395.
[111] S.K. Ramasahayam, U.B. Nasini, A.U. Shaikh, T. Viswanathan, Novel tannin-based Si, P co-doped carbon for supercapacitor applications, J. Power Sources 275 (2015) 835–844.
[112] W. Gu, M. Sevilla, A. Magasinski, A.B. Fuertes, G. Yushin, Sulfur-containing activated carbons with greatly reduced content of bottle neck pores for double-layer capacitors: a case study for pseudocapacitance detection, Energy Environ. Sci. 6 (8) (2013) 2465.
[113] J. Zhou, J. Lian, L. Hou, J. Zhang, H. Gou, M. Xia, et al., Ultrahigh volumetric capacitance and cyclic stability of fluorine and nitrogen co-doped carbon microspheres, Nat. Commun. 6 (2015) 8503.
[114] F. Zhou, H. Huang, C. Xiao, S. Zheng, X. Shi, J. Qin, et al., Electrochemically scalable production of fluorine-modified graphene for flexible and high-energy ionogel-based microsupercapacitors, J. Am. Chem. Soc. 140 (26) (2018) 8198–8205.
[115] S. Huang, Y. Li, Y. Feng, H. An, P. Long, C. Qin, et al., Nitrogen and fluorine co-doped graphene as a high-performance anode material for lithium-ion batteries, J. Mater. Chem. 3 (46) (2015) 23095–23105.
[116] Z.S. Wu, A. Winter, L. Chen, Y. Sun, A. Turchanin, X. Feng, et al., Three-dimensional nitrogen and boron co-doped graphene for high-performance all-solid-state supercapacitors, Adv. Mater. 24 (37) (2012) 5130–5135.
[117] Y. Yang, X. Hou, C. Ding, J.-L. Lan, Y. Yu, X. Yang, Eco-friendly fabricated nonporous carbon nanofibers with high volumetric capacitance: improving rate performance by tri-dopants of nitrogen, phosphorus, and silicon, Inorganic Chemistry Frontiers 4 (12) (2017) 2024–2032.
[118] G. Wang, X. Sun, F. Lu, H. Sun, M. Yu, W. Jiang, et al., Flexible pillared graphene-paper electrodes for high-performance electrochemical supercapacitors, Small 8 (3) (2012) 452–459.
[119] X. Lu, M. Yu, G. Wang, Y. Tong, Y. Li, Flexible solid-state supercapacitors: design, fabrication and applications, Energy Environ. Sci. 7 (7) (2014) 2160.
[120] R. Yuksel, Z. Sarioba, A. Cirpan, P. Hiralal, H.E. Unalan, Transparent and flexible supercapacitors with single walled carbon nanotube thin film electrodes, ACS Appl. Mater. Interfaces 6 (17) (2014) 15434–15439.
[121] H. Luo, P. Xiong, J. Xie, Z. Yang, Y. Huang, J. Hu, et al., Uniformly dispersed freestanding carbon nanofiber/graphene electrodes made by a scalable biological method for high-performance flexible supercapacitors, Adv. Funct. Mater. 28 (48) (2018) 1803075.
[122] S. He, W. Chen, High performance supercapacitors based on three-dimensional ultralight flexible manganese oxide nanosheets/carbon foam composites, J. Power Sources 262 (2014) 391–400.
[123] J. Han, Q. Ding, C. Mei, Q. Wu, Y. Yue, X. Xu, An intrinsically self-healing and biocompatible electroconductive hydrogel based on nanostructured nanocellulose-polyaniline complexes embedded in a viscoelastic polymer network towards flexible conductors and electrodes, Electrochim. Acta 318 (2019) 660–672.
[124] S. Zhou, G. Zhou, S. Jiang, P. Fan, H. Hou, Flexible and refractory tantalum carbide-carbon electrospun nanofibers with high modulus and electric conductivity, Mater. Lett. 200 (2017) 97–100.
[125] H.E. Shui-Jian, W. Chen, Progresses of self-supported supercapacitor electrode materials based on carbon substrates, Journal of Electrochemistry 21 (6) (2015) 518–533.
[126] S.J. He, W. Chen, Application of biomass-derived flexible carbon cloth coated with MnO2 nanosheets in supercapacitors, J. Power Sources 294 (2015) 150–158.
[127] C. Cheng, S. He, C. Zhang, C. Du, W. Chen, High-performance supercapacitor fabricated from 3D free-standing hierarchical carbon foam-supported two dimensional porous thin carbon nanosheets, Electrochim. Acta 290 (2018) 98–108.
[128] B.N.M. Dolah, M. Deraman, M.A.R. Othman, R. Farma, E. Taer, Awitdrus, et al., A method to produce binderless supercapacitor electrode monoliths from biomass carbon and carbon nanotubes, Mater. Res. Bull. 60 (2014) 10–19.
[129] P.X. Li, E.Z. Shi, Y.B. Yang, Y.Y. Shang, Q.Y. Peng, S.T. Wu, et al., Carbon nanotube-polypyrrole core-shell sponge and its application as highly compressible supercapacitor electrode, Nano Research 7 (2) (2014) 209–218.
[130] S. He, W. Chen, Application of biomass-derived flexible carbon cloth coated with MnO 2 nanosheets in supercapacitors, J. Power Sources 294 (2015) 150–158.
[131] N. Iqbal, X. Wang, A.A. Babar, G. Zainab, J. Yu, B. Ding, Flexible Fe3O4@Carbon nanofibers hierarchically assembled with MnO2 particles for high-performance supercapacitor electrodes, Sci. Rep. 7 (1) (2017) 15153.
[132] N. Iqbal, X. Wang, A.A. Babar, J. Yan, J. Yu, S.-J. Park, et al., Polyaniline enriched flexible carbon nanofibers with core-shell structure for high-performance wearable supercapacitors, Advanced Materials Interfaces 4 (24) (2017) 1700855.
[133] L. Kou, T. Huang, B. Zheng, Y. Han, X. Zhao, K. Gopalsamy, et al., Coaxial wet-spun yarn supercapacitors for high-energy density and safe wearable electronics, Nat. Commun. 5 (2014) 3754.
[134] T. Huang, S. Cai, H. Chen, Y. Jiang, S. Wang, C. Gao, Continuous fabrication of the graphene-confined polypyrrole film for cycling stable supercapacitors, J. Mater. Chem. 5 (18) (2017) 8255–8260.
[135] Q. Meng, H. Wu, Y. Meng, K. Xie, Z. Wei, Z. Guo, High-performance all-carbon yarn micro-supercapacitor for an integrated energy system, Adv. Mater. 26

(24) (2014) 4100–4106.
[136] M. Mo, C. Chen, H. Gao, M. Chen, D. Li, Wet-spinning assembly of cellulose nanofibers reinforced graphene/polypyrrole microfibers for high performance fiber-shaped supercapacitors, Electrochim. Acta 269 (2018) 11–20.
[137] P. Du, X. Hu, C. Yi, H.C. Liu, P. Liu, H.-L. Zhang, et al., Self-powered electronics by integration of flexible solid-state graphene-based supercapacitors with high performance perovskite hybrid solar cells, Adv. Funct. Mater. 25 (16) (2015) 2420–2427.
[138] Y. Yu, Y. Zhai, H. Liu, L. Li, Single-layer MnO 2 nanosheets: from controllable synthesis to free-standing film for flexible supercapacitors, Mater. Lett. 176 (2016) 33–37.
[139] Y. Yu, J. Zhong, W. Sun, R. Kumar, N. Koratkar, Solid-state hybrid fibrous supercapacitors produced by dead-end tube membrane ultrafiltration, Adv. Funct. Mater. 27 (24) (2017) 1606461.
[140] H.C. Tang, C. Yang, Z.Y. Lin, Q.H. Yang, F.Y. Kang, C.P. Wong, Electrospray-deposition of graphene electrodes: a simple technique to build high-performance supercapacitors, Nanoscale 7 (20) (2015) 9133–9139.
[141] J. Edberg, O. Inganäs, I. Engquist, M. Berggren, Boosting the capacity of all-organic paper supercapacitors using wood derivatives, J. Mater. Chem. 6 (1) (2018) 145–152.
[142] M. Hu, T. Hu, R. Cheng, J. Yang, C. Cui, C. Zhang, et al., MXene-coated silk-derived carbon cloth toward flexible electrode for supercapacitor application, J. Energy. Chem. 27 (1) (2018) 161–166.
[143] C.X. Hu, S.J. He, S.H. Jiang, S.L. Chen, H.Q. Hou, Natural source derived carbon paper supported conducting polymer nanowire arrays for high performance supercapacitors, RSC Adv. 5 (19) (2015) 14441–14447.
[144] G. Yu, X. Xie, L. Pan, Z. Bao, Y. Cui, Hybrid nanostructured materials for high-performance electrochemical capacitors, Nano Energy 2 (2) (2013) 213–234.
[145] C. Lai, Z. Zhou, L. Zhang, X. Wang, Q. Zhou, Y. Zhao, et al., Free-standing and mechanically flexible mats consisting of electrospun carbon nanofibers made from a natural product of alkali lignin as binder-free electrodes for high-performance supercapacitors, J. Power Sources 247 (2014) 134–141.
[146] S.C. Li, B.C. Hu, Y.W. Ding, H.W. Liang, C. Li, Z.Y. Yu, et al., Wood-derived ultrathin carbon nanofiber aerogels, Angew. Chem. Int. Ed. 57 (24) (2018) 7085–7090.
[147] X. Wang, W. Zhang, M. Chen, X. Zhou, Electrospun enzymatic hydrolysis lignin-based carbon nanofibers as binder-free supercapacitor electrodes with high performance, Polymers 10 (12) (2018) 1306.
[148] L. Wang, G. Zhang, X. Zhang, H. Shi, W. Zeng, H. Zhang, et al., Porous ultrathin carbon nanobubbles formed carbon nanofiber webs for high-performance flexible supercapacitors, J. Mater. Chem. 5 (28) (2017) 14801–14810.
[149] M. Yu, Y. Han, Y. Li, J. Li, L. Wang, Polypyrrole-anchored cattail biomass-derived carbon aerogels for high performance binder-free supercapacitors, Carbohydr. Polym. 199 (2018) 555–562.
[150] L. Basiricò, G. Lanzara, A monolithic functional film of nanotubes/cellulose/ionic liquid for high performance supercapacitors, J. Power Sources 271 (2014) 589–596.
[151] L.Z. Fan, Y.S. Hu, J. Maier, P. Adelhelm, B. Smarsly, M. Antonietti, High electroactivity of polyaniline in supercapacitors by using a hierarchically porous carbon monolith as a support, Adv. Funct. Mater. 17 (16) (2007) 3083–3087.
[152] S. Zhu, P.-L. Taberna, N. Zhao, P. Simon, Salt-template synthesis of mesoporous carbon monolith for ionogel-based supercapacitors, Electrochem. Commun. 96 (2018) 6–10.
[153] J. Han, H. Wang, Y. Yue, C. Mei, J. Chen, C. Huang, et al., A self-healable and highly flexible supercapacitor integrated by dynamically cross-linked electro-conductive hydrogels based on nanocellulose-templated carbon nanotubes embedded in a viscoelastic polymer network, Carbon 149 (2019) 1–18.
[154] Q. Zheng, A. Kvit, Z. Cai, Z. Ma, S. Gong, A freestanding cellulose nanofibril–reduced graphene oxide–molybdenum oxynitride aerogel film electrode for all-solid-state supercapacitors with ultrahigh energy density, J. Mater. Chem. 5 (24) (2017) 12528–12541.
[155] H. Huang, X. Zeng, W. Li, H. Wang, Q. Wang, Y. Yang, Reinforced conducting hydrogels prepared from the in situ polymerization of aniline in an aqueous solution of sodium alginate, J. Mater. Chem. 2 (39) (2014) 16516–16522.
[156] J. Le Bideau, L. Viau, Vioux A. Ionogels, Ionic liquid based hybrid materials, Chem. Soc. Rev. 40 (2) (2011) 907–925.
[157] Y. Zhang, F. Wang, H. Zhu, L. Zhou, X. Zheng, X. Li, et al., Preparation of nitrogen-doped biomass-derived carbon nanofibers/graphene aerogel as a binder-free electrode for high performance supercapacitors, Appl. Surf. Sci. 426 (2017) 99–106.
[158] T. Liu, W.-L. Song, L.-Z. Fan, Alcohol-dependent environments for fabricating graphene aerogels toward supercapacitors, Electrochim. Acta 173 (2015) 1–6.
[159] G. Ma, J. Li, K. Sun, H. Peng, J. Mu, Z. Lei, High performance solid-state supercapacitor with PVA–KOH–K3[Fe(CN)6] gel polymer as electrolyte and separator, J. Power Sources 256 (2014) 281–287.
[160] Q. Zheng, Z. Cai, Z. Ma, S. Gong, Cellulose nanofibril/reduced graphene oxide/carbon nanotube hybrid aerogels for highly flexible and all-solid-state supercapacitors, ACS Appl. Mater. Interfaces 7 (5) (2015) 3263–3271.
[161] W.L. Song, K. Song, L.Z. Fan, A versatile strategy toward binary three-dimensional architectures based on engineering graphene aerogels with porous carbon fabrics for supercapacitors, ACS Appl. Mater. Interfaces 7 (7) (2015) 4257–4264.
[162] W.J. Ma, M.J. Zhang, Z.C. Liu, M.M. Kang, C.B. Huang, G.D. Fu, Fabrication of highly durable and robust superhydrophobic-superoleophilic nanofibrous membranes based on a fluorine-free system for efficient oil/water separation, J. Membr. Sci. 570 (2019) 303–313.
[163] W.J. Ma, Z.F. Guo, J.T. Zhao, Q. Yu, F. Wang, J.Q. Han, et al., Polyimide/cellulose acetate core/shell electrospun fibrous membranes for oil-water separation, Separ. Purif. Technol. 177 (2017) 71–85.
[164] W.J. Ma, S.K. Samal, Z.C. Liu, R.H. Xiong, S.C. De Smedt, B. Bhushan, et al., Dual pH- and ammonia-vapor-responsive electrospun nanofibrous membranes for oil-water separations, J. Membr. Sci. 537 (2017) 128–139.
[165] M.M. Zhu, D.W. Hua, H. Pan, F. Wang, B. Manshian, S.J. Soenen, et al., Green electrospun and crosslinked poly(vinyl alcohol)/poly(acrylic acid) composite membranes for antibacterial effective air filtration, J. Colloid Interface Sci. 511 (2018) 411–423.
[166] M.M. Zhu, J.Q. Han, F. Wang, W. Shao, R.H. Xiong, Q.L. Zhang, et al., Electrospun nanofibers membranes for effective air filtration, Macromol. Mater. Eng. 302 (1) (2017) 27.
[167] S. Chen, S. He, H. Hou, Electrospinning technology for applications in supercapacitors, Curr. Org. Chem. 17 (13) (2013) 1402–1410.
[168] Z. Li, J-w Zhang, L-g Yu, J-w Zhang, Electrospun porous nanofibers for electrochemical energy storage, J. Mater. Sci. 52 (11) (2017) 6173–6195.
[169] Q. Li, L. Deng, J.-K. Kim, Y.Q. Zhu, S.M. Holmes, M. Perez-Page, et al., Growth of carbon nanotubes on electrospun cellulose fibers for high performance supercapacitors, J. Electrochem. Soc. 164 (13) (2017) A3220–A3228.
[170] J. Miao, M. Miyauchi, T.J. Simmons, J.S. Dordick, R.J. Linhardt, Electrospinning of nanomaterials and applications in electronic components and devices, J. Nanosci. Nanotechnol. 10 (9) (2010) 5507–5519.
[171] W.J. Ma, M.J. Zhang, Z.C. Liu, C.B. Huang, G.D. Fu, Nature- inspired creation of a robust free- standing electrospun nanofibrous membrane for efficient oil-water separation, Environ-Sci Nano. 5 (12) (2018) 2909–2920.
[172] W.J. Ma, J.T. Zhao, O. Oderinde, J.Q. Han, Z.C. Liu, B.H. Gao, et al., Durable superhydrophobic and superoleophilic electrospun nanofibrous membrane for oil-water emulsion separation, J. Colloid Interface Sci. 532 (2018) 12–23.
[173] X. Ma, P. Kolla, Y. Zhao, A.L. Smirnova, H. Fong, Electrospun lignin-derived carbon nanofiber mats surface-decorated with MnO 2 nanowhiskers as binder-free supercapacitor electrodes with high performance, J. Power Sources 325 (2016) 541–548.
[174] B. Vidyadharan, Misnon II, J. Ismail, M.M. Yusoff, R. Jose, High performance asymmetric supercapacitors using electrospun copper oxide nanowires anode, J. Alloy. Comp. 633 (2015) 22–30.
[175] D.W. Hua, Z.C. Liu, F. Wang, B.H. Gao, F. Chen, Q.L. Zhang, et al., pH responsive polyurethane (core) and cellulose acetate phthalate (shell) electrospun fibers for intravaginal drug delivery, Carbohydr. Polym. 151 (2016) 1240–1244.
[176] R. Zhang, L. Wang, J. Zhao, S.W. Guo, Effects of sodium alginate on the composition, morphology, and electrochemical properties of electrospun carbon nanofibers as electrodes for supercapacitors, ACS Sustain. Chem. Eng. 7 (1) (2019) 632–640.
[177] Q. Li, Y.Q. Zhu, S.J. Eichhorn, Structural supercapacitors using a solid resin electrolyte with carbonized electrospun cellulose/carbon nanotube electrodes, J. Mater. Sci. 53 (20) (2018) 14598–14607.
[178] M. Xu, M. Wang, H. Xu, H. Xue, H. Pang, Electrospun-Technology-derived high-performance electrochemical energy storage devices, Chem. Asian J. 11 (21) (2016) 2967–2995.
[179] M.J. Zhang, W.J. Ma, S.T. Wu, G.S. Tang, J.X. Cui, Q.L. Zhang, et al., Electrospun frogspawn structured membrane for gravity-driven oil-water separation, J. Colloid Interface Sci. 547 (2019) 136–144.
[180] G. Duan, H. Fang, C. Huang, S. Jiang, H. Hou, Microstructures and mechanical properties of aligned electrospun carbon nanofibers from binary composites of polyacrylonitrile and polyamic acid, J. Mater. Sci. 53 (21) (2018) 15096–15106.
[181] H. Xu, S. Jiang, C. Ding, Y. Zhu, J. Li, H. Hou, High strength and high breaking load of single electrospun polyimide microfiber from water soluble precursor, Mater. Lett. 201 (2017) 82–84.
[182] G. Duan, S. Liu, S. Jiang, H. Hou, High-performance polyamide-imide films and electrospun aligned nanofibers from an amide-containing diamine, J. Mater. Sci. 54 (8) (2019) 6719–6727.
[183] S. Peng, G. Jin, L. Li, K. Li, M. Srinivasan, S. Ramakrishna, et al., Multi-functional electrospun nanofibres for advances in tissue regeneration, energy conversion & storage, and water treatment, Chem. Soc. Rev. 45 (5) (2016) 1225–1241.
[184] J. Zhang, P. Chen, B.H.L. Oh, M.B. Chan-Park, High capacitive performance of flexible and binder-free graphene–polypyrrole composite membrane based on in situ reduction of graphene oxide and self-assembly, Nanoscale 5 (20) (2013) 9860.
[185] Q. Wu, Y. Xu, Z. Yao, A. Liu, G. Shi, Supercapacitors based on flexible graphene/polyaniline nanofiber composite films, ACS Nano 4 (4) (2010) 1963–1970.
[186] R. Liu, L. Ma, S. Huang, J. Mei, J. Xu, G. Yuan, Large areal mass, flexible and freestanding polyaniline/bacterial cellulose/graphene film for high-performance supercapacitors, RSC Adv. 6 (109) (2016) 107426–107432.
[187] L.N. Ma, R. Liu, H.J. Niu, F. Wang, L. Liu, Y.D. Huang, Freestanding conductive film based on polypyrrole/bacterial cellulose/graphene paper for flexible supercapacitor: large areal mass exhibits excellent areal capacitance, Electrochim. Acta 222 (2016) 429–437.
[188] H. Song, J. Fu, K. Ding, C. Huang, K. Wu, X. Zhang, et al., Flexible Nb2O5 nanowires/graphene film electrode for high-performance hybrid Li-ion

supercapacitors, J. Power Sources 328 (2016) 599–606.
[189] N. Li, X. Li, C. Yang, F. Wang, J. Li, H. Wang, et al., Fabrication of a flexible free-standing film electrode composed of polypyrrole coated cellulose nanofibers/multi-walled carbon nanotubes composite for supercapacitors, RSC Adv. 6 (89) (2016) 86744–86751.
[190] S. Hu, S. Zhang, N. Pan, Y.-L. Hsieh, High energy density supercapacitors from lignin derived submicron activated carbon fibers in aqueous electrolytes, J. Power Sources 270 (2014) 106–112.
[191] Q. Xie, S. Wu, Y. Zhang, P. Zhao, Nitrogen-enriched flexible porous carbon/graphene composite cloth as free-standing electrodes for high performance aqueous supercapacitors, J. Electroanal. Chem. 801 (2017) 57–64.
[192] K. Song, H. Ni, L.-Z. Fan, Flexible graphene-based composite films for supercapacitors with tunable areal capacitance, Electrochim. Acta 235 (2017) 233–241.
[193] Y. Liu, Z. Shi, Y. Gao, W. An, Z. Cao, J. Liu, Biomass-swelling assisted synthesis of hierarchical porous carbon fibers for supercapacitor electrodes, ACS Appl. Mater. Interfaces 8 (42) (2016) 28283–28290.
[194] J. Du, L. Liu, Z. Hu, Y. Yu, Y. Zhang, S. Hou, et al., Raw-cotton-derived N-doped carbon fiber aerogel as an efficient electrode for electrochemical capacitors, ACS Sustain. Chem. Eng. 6 (3) (2018) 4008–4015.
[195] S. He, C. Zhang, C. Du, C. Cheng, W. Chen, High rate-performance supercapacitor based on nitrogen-doped hollow hexagonal carbon nanoprism arrays with ultrathin wall thickness in situ fabricated on carbon cloth, J. Power Sources 434 (2019) 226701.
[196] L. Li, Q. Zhong, N.D. Kim, G. Ruan, Y. Yang, C. Gao, et al., Nitrogen-doped carbonized cotton for highly flexible supercapacitors, Carbon 105 (2016) 260–267.
[197] W.-L. Song, X. Li, L.-Z. Fan, Biomass derivative/graphene aerogels for binder-free supercapacitors, Energy Storage Materials 3 (2016) 113–122.
[198] M. Rana, S. Asim, B. Hao, S. Yang, P.-C. Ma, Carbon nanotubes on highly interconnected carbonized cotton for flexible and light-weight energy storage, Advanced Sustainable Systems 1 (5) (2017) 1700022.
[199] Y.-M. Fan, W.-L. Song, X. Li, L.-Z. Fan, Assembly of graphene aerogels into the 3D biomass-derived carbon frameworks on conductive substrates for flexible supercapacitors, Carbon 111 (2017) 658–666.
[200] X. Hao, J. Wang, B. Ding, Y. Wang, Z. Chang, H. Dou, et al., Bacterial-cellulose-derived interconnected meso-microporous carbon nanofiber networks as binder-free electrodes for high-performance supercapacitors, J. Power Sources 352 (2017) 34–41.
[201] Y. Chang, L. Zhou, Z. Xiao, J. Liang, D. Kong, Z. Li, et al., Embedding reduced graphene oxide in bacterial cellulose-derived carbon nanofibril networks for supercapacitors, ChemElectroChem 4 (10) (2017) 2448–2452.
[202] L.F. Chen, Z.H. Huang, H.W. Liang, W.T. Yao, Z.Y. Yu, S.H. Yu, Flexible all-solid-state high-power supercapacitor fabricated with nitrogen-doped carbon nanofiber electrode material derived from bacterial cellulose, Energy Environ. Sci. 6 (11) (2013) 3331–3338.
[203] R. Liu, L. Pan, L. Wan, D. Wu, An evaporation-induced tri-consistent assembly route towards nitrogen-doped carbon microfibers with ordered mesopores for high performance supercapacitors, Phys. Chem. Chem. Phys. : Phys. Chem. Chem. Phys. 17 (6) (2015) 4724–4729.
[204] R. Liu, L. Pan, J. Jiang, X. Xi, X. Liu, D. Wu, Nitrogen-doped carbon microfiber with wrinkled surface for high performance supercapacitors, Sci. Rep. 6 (2016) 21750.
[205] X. Li, J. Zhao, Z. Cai, F. Ge, A dyeing-induced heteroatom-co-doped route toward flexible carbon electrode derived from silk fabric, J. Mater. Sci. 53 (10) (2018) 7735–7743.
[206] X. Li, J. Zhao, Z. Cai, F. Ge, Free-standing carbon electrode materials with three-dimensional hierarchically porous structure derived from waste dyed silk fabrics, Mater. Res. Bull. 107 (2018) 355–360.
[207] B.-X. Zou, Y. Gao, B. Liu, Y. Yu, Y. Lu, Three dimensional heteroatom-doped carbon composite film for flexible solid-state supercapacitors, RSC Adv. 6 (6) (2016) 4483–4489.
[208] B.-X. Zou, Y. Wang, X. Huang, Y. Lu, Hierarchical N- and O-doped porous carbon composites for high-performance supercapacitors, J. Nanomater. 2018 (2018) 1–12.
[209] R. Berenguer, F.J. Garcia-Mateos, R. Ruiz-Rosas, D. Cazorla-Amoros, E. Morallon, J. Rodriguez-Mirasol, et al., Biomass-derived binderless fibrous carbon electrodes for ultrafast energy storage, Green Chem. 18 (6) (2016) 1506–1515.
[210] C.D. Tran, H.C. Ho, J.K. Keum, J. Chen, N.C. Gallego, A.K. Naskar, Sustainable energy-storage materials from lignin-graphene nanocomposite-derived porous carbon film, Energy Technol. 5 (11) (2017) 1927–1935.
[211] P. Schlee, O. Hosseinaei, D. Baker, A. Landmér, P. Tomani, M.J. Mostazo-López, et al., From waste to wealth: from Kraft lignin to free-standing supercapacitors, Carbon 145 (2019) 470–480.
[212] P. Schlee, S. Herou, R. Jervis, P.R. Shearing, D.J.L. Brett, D. Baker, et al., Free-standing supercapacitors from Kraft lignin nanofibers with remarkable volumetric energy density, Chem. Sci. 10 (10) (2019) 2980–2988.
[213] R.A. Perera Jayawickramage, J.P. Ferraris, High performance supercapacitors using lignin based electrospun carbon nanofiber electrodes in ionic liquid electrolytes, Nanotechnology 30 (15) (2019) 155402.
[214] H. Li, D. Yuan, C. Tang, S. Wang, J. Sun, Z. Li, et al., Lignin-derived interconnected hierarchical porous carbon monolith with large areal/volumetric capacitances for supercapacitor, Carbon 100 (2016) 151–157.
[215] C. Ma, J. Chen, Q. Fan, J. Guo, W. Liu, E. Cao, et al., Preparation and one-step activation of nanoporous ultrafine carbon fibers derived from polyacrylonitrile/cellulose blend for used as supercapacitor electrode, J. Mater. Sci. 53 (6) (2017) 4527–4539.
[216] Q. Fan, C. Ma, L. Wu, C. Wei, H. Wang, Y. Song, et al., Preparation of cellulose acetate derived carbon nanofibers by ZnCl2 activation as a supercapacitor electrode, RSC Adv. 9 (12) (2019) 6419–6428.
[217] Y. Zhong, T. Shi, Y. Huang, S. Cheng, G. Liao, Z. Tang, One-step synthesis of porous carbon derived from starch for all-carbon binder-free high-rate supercapacitor, Electrochim. Acta 269 (2018) 676–685.
[218] Y.K. Kim, S.I. Cha, S.H. Hong, Y.J. Jeong, A new hybrid architecture consisting of highly mesoporous CNT/carbon nanofibers from starch, J. Mater. Chem. 22 (38) (2012) 20554.
[219] X.-F. Jiang, X.-B. Wang, P. Dai, X. Li, Q. Weng, X. Wang, et al., High-throughput fabrication of strutted graphene by ammonium-assisted chemical blowing for high-performance supercapacitors, Nano Energy 16 (2015) 81–90.
[220] Wei Lu, NN, Yushin Gleb, Lithographically patterned thin activated carbon films as a new technology platform for on-chip devices, ACS Nano 7 (8) (2013) 6498–6506.
[221] N. Díez, C. Botas, E. Goikolea, D. Carriazo, Macroporous carbon monoliths derived from phloroglucinol–sucrose resins as binder-free thick electrodes for supercapacitors, J. Mater. Sci. 52 (19) (2017) 11191–11200.
[222] A. Kurniawan, L.K. Ong, F. Kurniawan, C.X. Lin, F.E. Soetaredjo, X.S. Zhao, et al., Easy approach to synthesize N/P/K co-doped porous carbon microfibers from cane molasses as a high performance supercapacitor electrode material, RSC Adv. 4 (66) (2014) 34739–34750.
[223] X. Tong, H. Zhuo, S. Wang, L. Zhong, Y. Hu, X. Peng, et al., A new strategy to tailor the structure of sustainable 3D hierarchical porous N-self-doped carbons from renewable biomass for high-performance supercapacitors and CO2 capture, RSC Adv. 6 (41) (2016) 34261–34270.
[224] X.F. Zhang, J.Q. Zhao, X. He, Q.Y. Li, C.H. Ao, T. Xia, et al., Mechanically robust and highly compressible electrochemical supercapacitors from nitrogen-doped carbon aerogels, Carbon 127 (2018) 236–244.
[225] Z.J. Tang, Z.X. Pei, Z.F. Wang, H.F. Li, J. Zeng, Z.H. Ruan, et al., Highly anisotropic, multichannel wood carbon with optimized heteroatom doping for supercapacitor and oxygen reduction reaction, Carbon 130 (2018) 532–543.
[226] P. Hu, D. Meng, G. Ren, R. Yan, X. Peng, Nitrogen-doped mesoporous carbon thin film for binder-free supercapacitor, Applied Materials Today 5 (2016) 1–8.
[227] T. Purkait, G. Singh, M. Singh, D. Kumar, R.S. Dey, Large area few-layer graphene with scalable preparation from waste biomass for high-performance supercapacitor, Sci. Rep. 7 (1) (2017) 15239.
[228] T.-D. Nguyen, K.E. Shopsowitz, M.J. MacLachlan, Mesoporous nitrogen-doped carbon from nanocrystalline chitin assemblies, J. Mater. Chem. 2 (16) (2014) 5915.
[229] Y. Li, Q. Zhang, J. Zhang, L. Jin, X. Zhao, T. Xu, A top-down approach for fabricating free-standing bio-carbon supercapacitor electrodes with a hierarchical structure, Sci. Rep. 5 (2015) 14155.
[230] N. Kostoglou, C. Koczwara, C. Prehal, V. Terziyska, B. Babic, B. Matovic, et al., Nanoporous activated carbon cloth as a versatile material for hydrogen adsorption, selective gas separation and electrochemical energy storage, Nano Energy 40 (2017) 49–64.
[231] T. Lin, F. Liu, F. Xu, H. Bi, Y. Du, Y. Tang, et al., Superelastic few-layer carbon foam made from natural cotton for all-solid-state electrochemical capacitors, ACS Appl. Mater. Interfaces 7 (45) (2015) 25306–25312.
[232] G.P. Mane, S.N. Talapaneni, C. Anand, S. Varghese, H. Iwai, Q. Ji, et al., Preparation of highly ordered nitrogen-containing mesoporous carbon from a gelatin biomolecule and its excellent sensing of acetic acid, Adv. Funct. Mater. 22 (17) (2012) 3596–3604.
[233] Y. Liang, D. Wu, R. Fu, Carbon microfibers with hierarchical porous structure from electrospun fiber-like natural biopolymer, Sci. Rep. 3 (2013) 1119.
[234] Y.S. Yun, M.E. Lee, M.J. Joo, H.-J. Jin, High-performance supercapacitors based on freestanding carbon-based composite paper electrodes, J. Power Sources 246 (2014) 540–547.
[235] V. Sahu, S. Grover, B. Tulachan, M. Sharma, G. Srivastava, M. Roy, et al., Heavily nitrogen doped, graphene supercapacitor from silk cocoon, Electrochim. Acta 160 (2015) 244–253.
[236] X. Wang, Y. Zhang, C. Zhi, X. Wang, D. Tang, Y. Xu, et al., Three-dimensional strutted graphene grown by substrate-free sugar blowing for high-power-density supercapacitors, Nat. Commun. 4 (2013) 2905.
[237] V. Barbera, S. Guerra, L. Brambilla, M. Maggio, A. Serafini, L. Conzatti, et al., Carbon papers and aerogels based on graphene layers and chitosan: direct preparation from high surface area graphite, Biomacromolecules 18 (12) (2017) 3978–3991.
[238] X. Zhang, Y. Jiao, L. Sun, L. Wang, A. Wu, H. Yan, et al., GO-induced assembly of gelatin toward stacked layer-like porous carbon for advanced supercapacitors, Nanoscale 8 (4) (2016) 2418–2427.
[239] L.-L. Zhang, H.-H. Li, Y.-H. Shi, C.-Y. Fan, X.-L. Wu, H.-F. Wang, et al., A novel layered sedimentary rocks structure of the oxygen-enriched carbon for ultrahigh-rate-performance supercapacitors, ACS Appl. Mater. Interfaces 8 (6) (2016) 4233–4241.
[240] B. Xu, S. Hou, F. Zhang, G. Cao, M. Chu, Y. Yang, Nitrogen-doped mesoporous carbon derived from biopolymer as electrode material for supercapacitors, J. Electroanal. Chem. 712 (2014) 146–150.
[241] B.K. Baik, S.E. Ullrich, Barley for food: characteristics, improvement, and

renewed interest, J. Cereal Sci. 48 (2) (2008) 233–242.
[242] T.J. Anderson, B.P. Lamsal, Zein extraction from corn, corn products, and coproducts and modifications for various applications: a review, Cereal Chem. 88 (2) (2011) 159–173.
[243] L.F. Chen, X.D. Zhang, H.W. Liang, M.G. Kong, Q.F. Guan, P. Chen, et al., Synthesis of nitrogen-doped porous carbon nanofibers as an efficient electrode material for supercapacitors, ACS Nano 6 (8) (2012) 7092–7102.
[244] K. Moomand, L.T. Lim, Oxidative stability of encapsulated fish oil in electrospun zein fibres, Food Res. Int. 62 (2014) 523–532.
[245] Y.X. Wang, L.Y. Chen, Cellulose nanowhiskers and fiber alignment greatly improve mechanical properties of electrospun prolamin protein fibers, ACS Appl. Mater. Interfaces 6 (3) (2014) 1709–1718.
[246] Y.X. Wang, J.Q. Yang, L.Y. Chen, Convenient fabrication of electrospun prolamin protein delivery system with three-dimensional shapeability and resistance to fouling, ACS Appl. Mater. Interfaces 7 (24) (2015) 13422–13430.
[247] J. Yang, Y. Wang, J. Luo, L. Chen, Facile preparation of self-standing hierarchical porous nitrogen-doped carbon fibers for supercapacitors from plant protein–lignin electrospun fibers, ACS Omega 3 (4) (2018) 4647–4656.
[248] Y. Wang, J. Yang, R. Du, L. Chen, Transition metal ions enable the transition from electrospun prolamin protein fibers to nitrogen-doped freestanding carbon films for flexible supercapacitors, ACS Appl. Mater. Interfaces 9 (28) (2017) 23731–23740.